



Actual evapotranspiration in drylands derived from in-situ and satellite data: Assessing biophysical constraints

Monica García^{a,b,*}, Inge Sandholt^{a,b}, Pietro Ceccato^b, Marc Ridler^a, Eric Mougin^c, Laurent Kergoat^c, Laura Morillas^d, Franck Timouk^c, Rasmus Fensholt^a, Francisco Domingo^d

^a Institute of Geography, University of Copenhagen, Øster Voldgade 10, DK-1350 Copenhagen, Denmark

^b International Research Institute for Climate & Society, The Earth Institute, Columbia University, Lamont Campus, 61 Route 9W, Palisades, NY 10964-8000, USA

^c Géosciences Environnement Toulouse (UMR 5563 UPS-CNRS-IRD) Observatoire Midi-Pyrénées (OMP), Université de Toulouse, 18 Avenue Edouard Belin 31401 Toulouse Cedex 9, France

^d Desertification and Geocology Dept. Estación Experimental de Zonas Áridas (EEZA), Consejo Superior de Investigaciones Científicas, Crtra. de Sacramento s/n La Cañada de San Urbano, E-04120 Almería, Spain

ARTICLE INFO

Article history:

Received 8 May 2012

Received in revised form 10 December 2012

Accepted 14 December 2012

Available online 15 January 2013

Keywords:

Evapotranspiration

Surface temperature

Priestley–Taylor

Thermal inertia

MSG–SEVIRI

Water-limited ecosystems

MODIS

ABSTRACT

Improving regional estimates of actual evapotranspiration (λE) in water-limited regions located at climatic transition zones is critical. This study assesses an λE model (PT–JPL model) based on downscaling potential evapotranspiration according to multiple stresses at daily time-scale in two of these regions using MSG–SEVIRI (surface temperature and albedo) and MODIS products ($NDVI$, LAI and f_{PAR}). An open woody savanna in the Sahel (Mali) and a Mediterranean grassland (Spain) were selected as test sites with Eddy Covariance data used for evaluation. The PT–JPL model was modified to run at a daily time step and the outputs from eight algorithms differing in the input variables and also in the formulation of the biophysical constraints (stresses) were compared with the λE from the Eddy Covariance. Model outputs were also compared with other modeling studies at similar global dryland ecosystems.

The novelty of this paper is the computation of a key model parameter, the soil moisture constraint, relying on the concept of apparent thermal inertia (f_{SM-ATI}) computed with surface temperature and albedo observations. Our results showed that f_{SM-ATI} from both in-situ and satellite data produced satisfactory results for λE at the Sahelian savanna, comparable to parameterizations using field-measured Soil Water Content (SWC) with r^2 greater than 0.80. In the Mediterranean grasslands however, with much lower daily λE values, model results were not as good as in the Sahel ($r^2 = 0.57–0.31$) but still better than reported values from more complex models applied at the site such as the Two Source Model (TSM) or the Penman–Monteith Leuning model (PML).

PT–JPL-daily model with a soil moisture constraint based on apparent thermal inertia, f_{SM-ATI} offers great potential for regionalization as no field-calibrations are required and water vapor deficit estimates, required in the original version, are not necessary, being air temperature and the available energy ($Rn-G$) the only input variables required, apart from routinely available satellite products.

© 2012 Elsevier Inc. All rights reserved.

1. Introduction

Evapotranspiration (or latent heat flux expressed in energy terms, λE) represents 90% of the annual precipitation in water-limited regions which cover 40% of the Earth's surface (Glenn et al., 2007). In these regions there is a close link between carbon and water cycles (Baldocchi, 2008) where water availability is the main control for biological activity (Brogaard et al., 2005). λE rates also determine groundwater recharge (Huxman et al., 2005) and feedbacks to continental precipitation patterns (Huntington, 2006). The Sahel and the Mediterranean basin are both located in transitional climate regions and are thus

expected to be extremely sensitive to climate change (Giorgi & Lionello, 2008). The land surface is a strong amplifier on the inter-annual variability of the West African Monsoon leading to the observed persistency patterns (Nicholson, 2000; Taylor et al., 2011; Timouk et al., 2009). Therefore, improving estimates of temporal and spatial variations of λE is crucial for understanding land surface–atmosphere interactions and to improve hydrological and agricultural management (Yuan et al., 2010).

λE can be estimated at regional scales using remote sensing data. One way is to use models based on the bulk resistance equation for heat transfer (Brutsaert, 1982), relying on the difference between surface temperature (T_s) and air temperature (T_a) and the aerodynamic resistance to turbulent heat transport. In this case, λE is estimated indirectly as a residual of the surface energy balance equation (Anderson et al., 2007; Chehbouni et al., 1997). This approach circumvents the problem

* Corresponding author at: Institute of Geography, University of Copenhagen, Øster Voldgade 10, DK-1350 Copenhagen, Denmark. Tel.: +45 35322500; fax: +45 35322501.
E-mail address: Mg@geo.ku.dk (M. García).

of estimating soil and canopy surface resistances to water vapor, needed to compute λE , that tend to be more critical in λE modeling than aerodynamic resistances in dryland regions (Verhoef, 1998; Were et al., 2007). In those regions, two-source models treating the land surface as a composite of soil and vegetation elements with different temperatures, fluxes, and atmospheric coupling provide better results than single-source models (Anderson et al., 2007). However, despite the strong physical basis of two-source models (Kustas & Norman, 1999; Norman et al., 1995) their spatialization is difficult because the task of estimating aerodynamic resistances at instantaneous time scales is not trivial, requiring knowledge about atmospheric stability, several vegetation and soil parameters as well as meteorological data (Fisher et al., 2008). Further complications arise from the partition of T_s between soil and vegetation (Kustas & Norman, 1999) because the radiative surface temperature differs from the aerodynamic surface temperature especially over sparsely vegetated surfaces (Chehbouni et al., 1997).

A second group of models using remote sensing data directly solves the λE term using the Penman–Monteith (PM) combination equation. In this case, λE can be partitioned into soil and vegetation components (Leuning et al., 2008). With this approach, the challenge is to characterize the spatial and temporal variation in surface conductances to water vapor without using field calibration (Zhang et al., 2010). A simple way to estimate surface conductances is to use prescribed sets of parameters based on biome-type maps (Zhang et al., 2010). Other approaches perform optimization with field data but can lead to a lack of estimates over vast regions of the globe, such as the Sahel, due to the scarcity of field measurements (Yuan et al., 2010). One of the first attempts to characterize surface conductance without optimization proposed an empirical relationship with LAI derived from MODIS (Moderate Resolution Imaging Spectroradiometer) (Cleugh et al., 2007). Mu et al. (2007, 2011) refined this approach using the empirical multiplicative model proposed by (Jarvis, 1976) estimating moisture and temperature constraints on stomatal conductance and upscaling leaf stomatal conductance to canopy. Alternatively, Leuning et al. (2008) used a biophysical model for surface conductance based on Kelliher et al. (1995) method. However, this method required optimization with field data for g_{sx} , the maximum stomatal conductance of leaves, and for the soil water content. As both parameters were held constant along the year λE was overestimated at drier sites. To address this shortcoming, Zhang et al. (2008) introduced a variable-soil moisture fraction dependent on rainfall, and optimized g_{sx} using outputs from an annual water balance model or a Budyko-type model (Zhang et al., 2008, 2010). Although this represented a step-forward for operational applications, results at dry sites were still poorer than at more humid sites (Zhang et al., 2008, 2010).

A solution to overcome those parameterization problems using the Penman–Monteith equation, was the simplification proposed by Priestley and Taylor (1972) (PT) for equilibrium evapotranspiration over large regions by replacing the surface and aerodynamic resistance terms with an empirical multiplier α_{PT} (Zhang et al., 2009). The PT equation is theoretically less accurate than PM although uncertainties in parameter estimation using PM can result in higher errors (Fisher et al., 2008). Fisher et al. (2008) proposed a model based on PT to estimate monthly actual λE . The authors used biophysical constraints to reduce λE from a maximum potential value, λE_p , in response to multiple stresses. One advantage of this approach is that it does not require information regarding biome-type or calibration with field data. The modeling framework can be seen as conceptually similar to the so-called Production Efficiency Models (PEM) for estimating GPP (Gross Primary Productivity) (Houborg et al., 2009; Monteith, 1972; Potter et al., 1993; Verstraeten et al., 2006a) where maximum light use efficiency (ϵ) of conversion of absorbed energy f_{APAR} into carbon is reduced below its maximum potential due to environmental stresses. In fact, part of the formulation from the PT-JPL model has been introduced into some PEM models (Yuan et al., 2010). The main model assumption is that plants optimize their capacity for energy acquisition

in a way that changes in parallel with the physiological capacity for transpiration (Fisher et al., 2008; Nemani & Running, 1989). This idea is to some extent related to the hydrological equilibrium hypothesis stating that in water-limited natural systems, plants adjust canopy development to minimize water losses and maximize carbon gains (Eagleson, 1986) but applied over shorter time-scales. The modeling approach described above neglects the behavior of individual leaves and considers the canopy response to its environment in bulk for which it can be referred to as a top-down approach (Houborg et al., 2009). Top-down approaches use simpler scaling rules compared to bottom-up models that require detailed mechanistic descriptions of leaf-level processes up-scaled to the canopy (Schymanski et al., 2009). Although top-down approaches require less parameters than bottom-up approaches, they are subjected to a higher degree of empiricism with high uncertainty on the functional responses of ecosystem processes to environmental stresses (Yuan et al., 2010).

The use of global satellite vegetation products and meteorological gridded databases as input to top-down approaches based on the PM or the PT equations has made possible to obtain regional estimates of evapotranspiration (Mu et al., 2007). However, there are still limitations regarding the use of such databases. One hand, existing global climatic data sets interpolated from observations such as the Climatic Research Unit data set (CRU, University of East Anglia) are available on a monthly but not a daily basis (New et al., 2000). Moreover, data from reanalyses such as ECMWF (European Centre for Medium-Range Weather Forecasts) or NCEP/NCAR present coarse spatial resolutions ($\approx 1.25^\circ$) (Mu et al., 2007) being desirable to minimize the use of climatic data when possible.

On the other hand, PM and PT satellite-based approaches have taken advantage of optical remote sensing data to estimate vegetation properties but thermal remotely sensed data has been used only marginally and with coarse spatial resolution data such as the microwave AMSR-E at 0.25° (Miralles et al., 2011). Incorporation of longwave infrared thermal data at spatial resolutions of 1–3 km available from the MODIS (Moderate Resolution Imaging Spectroradiometer) or the SEVIRI (Spinning Enhanced Visible and Infrared Imager) sensors could help to track changes in surface conductance (Berni et al., 2009; Boegh et al., 2002), soil evaporation (Qiu et al., 2006), surface water deficit (Boulet et al., 2007; Moran et al., 1994) or soil water content (Gillies & Carlson, 1995; Nishida et al., 2003; Sandholt et al., 2002). In relation to soil moisture a promising approach is the mapping of soil moisture based on soil thermal inertia (Cai et al., 2007; Sobrino et al., 1998; Verstraeten et al., 2006b), following the early work of Price (1977) and Cracknell and Xue (1996).

The objective of this work was to adapt and evaluate a daily version of the PT-JPL model and introduce a new formulation for soil moisture based on the thermal inertia concept. The aim is to minimize the need for climatic reanalyses data by incorporating thermal remote sensing information in order to facilitate future model regionalization. The PT-JPL model in its original formulation has proven to be successful over 36 Fluxnet sites at monthly time scales, ranging from boreal to temperate and tropical ecosystems. However, none of those included semiarid vegetation with annual rainfall below 400 mm (Fisher et al., 2008, 2009). Model performance using in-situ and satellite data was compared with field data from Eddy Covariance systems at two semiarid sites: an open woody savannah in the Sahel (Mali) and Mediterranean tussock grassland (Spain). Finally, to place the results in the context of global drylands, model results were compared to published results from similar models using remote sensing at dryland savanna and grasslands sites across the globe.

2. Field sites and data

Two field sites (Fig. 1) have been used to test the model in semiarid conditions: an open woody savannah in Mali and tussock grassland in Spain. A general description of the sites is included in Table 1.

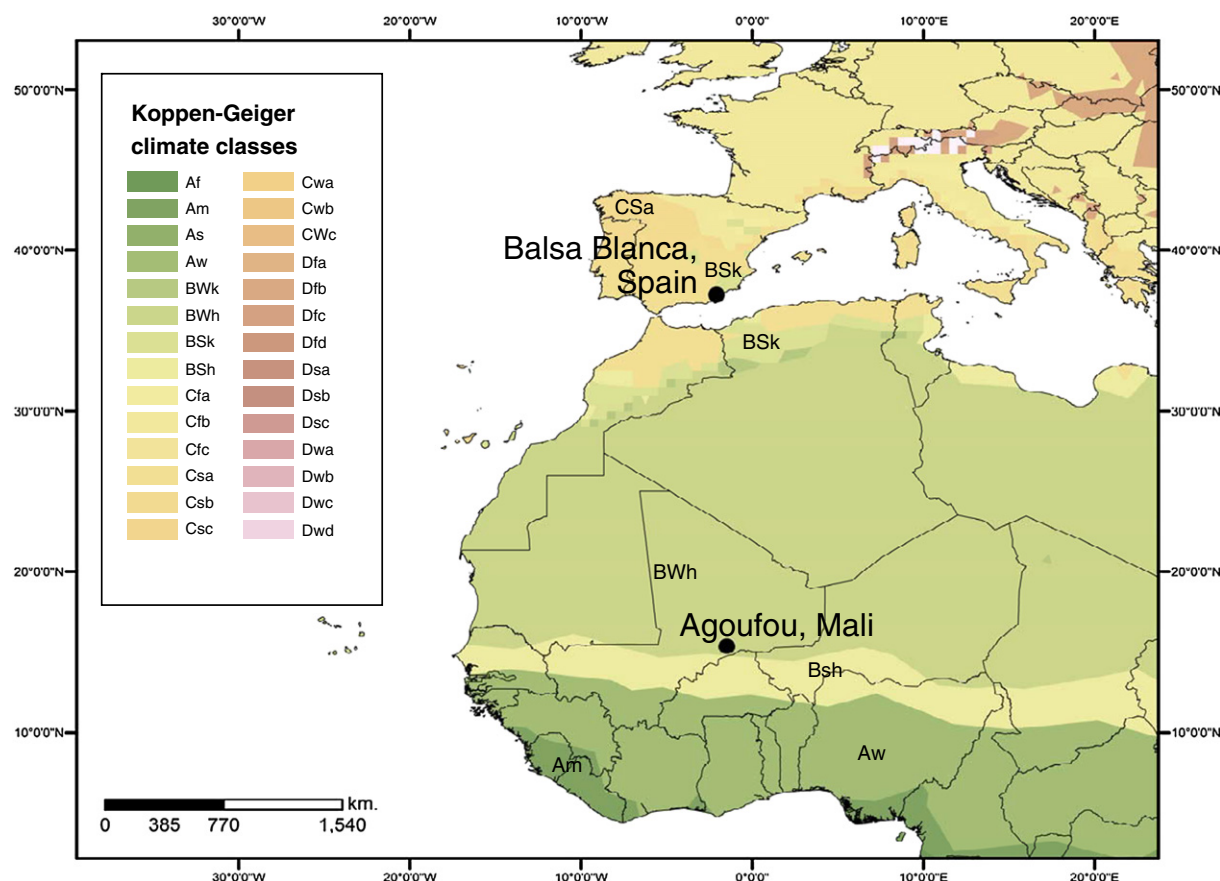


Fig. 1. Location of the two study sites: an open woody savanna (15.34°N, 1.48°W) in the Sahel (Agoufou site, Mali) and Mediterranean tussock grassland (36.94°N, 2.03°W) in Spain (Balsa Blanca site). The map with Köppen–Geiger climate classes (Kottek et al., 2006) overlaps country boundaries. The Mediterranean site presents cold semiarid climate (BSk) and the Sahelian site Arid desert hot climate (BWh).

2.1. Sahelian open woody savannah site

The Agoufou site is an open woody savannah, homogeneous over several kilometers, with trees representing less than 5% of vegetation cover. A comprehensive description of the site is provided by Mougin et al. (2009). The top 0–6 cm of the soil is 91% sand, 3.3% silt and 4.6% clay (de Rosnay et al., 2009). The region experiences a single rainy season with most precipitation falling between late June and mid September followed by a long dry season of around 8 months.

In-situ data for the 2007 growing season were provided by the African Monsoon Multidisciplinary Analyses (AMMA) project. Sensible heat flux was measured with sonic anemometers (CSAT) measuring the three vector components of the wind at 20 Hz. Latent heat fluxes were measured with the Eddy–Covariance system (Campbell CR3000 and CSAT3–LiCor7500, Campbell Scientific Inc. and Li-Cor Inc.). The four components of the net radiation were measured with a CNR1 (Kipp and Zonen CNR1, Delft, Holland).

Measurement height for the flux sensors is 2.2 m. Soil heat fluxes were computed from soil temperature measurements. See Timouk et al. (2009) for more details. Wind speed and direction (Vector A100R), land surface temperature (Everest 4000.4zl), air temperature and humidity (HMP 45C, Vaisala) and precipitation (Delta T, RG1) were also measured. Time domain reflectometry sensors (Campbell CS616, Campbell Scientific Inc., USA) measured volumetric Soil Water Content at several depths with the shallower probe, the one used in this work, located at 5 cm.

Leaf Area Index (LAI) and fractional cover were monitored approximately every 10 days during the 2007 growing season (DOY 184 to 269) along a 1 km long vegetation transect using hemispherical photographs. LAI was validated using destructive measurements (Mougin et al., 2009). Comparisons with MODIS LAI during three years produced $r^2 = 0.82$ and RMSE 0.26 (Mougin et al., 2009). The fraction of vegetation cover is 50%, with a maximum average height of 0.4 m for the herbaceous cover. A period starting prior and finishing after the rains was

Table 1

General characteristics of the two instrumented field sites in the Sahel region and in the Mediterranean basin.

Site name (location)	Vegetation type	Mean annual rainfall	Soil type	Dominant herbaceous species	Dominant woody species
Agoufou (Mali) (15.34°N, 1.48°W)	Open woody savannah	375 mm	Fixed dunes-Arenosol	<i>Cenchrus biflorus</i> , <i>Aristida mutabilis</i> , <i>Zornia glochidiata</i> , <i>Tragus berteronianus</i>	<i>Acacia raddiana</i> , <i>Acacia senegal</i> , <i>Combretum glutinosum</i> , <i>Balanites aegyptiaca</i> , <i>Leptadenia pyrotechnica</i>
Balsa Blanca (Spain) (36.94°N, 2.03°W)	Tussock grassland	370 mm	Calcium crusts-Mollic leptosol	<i>Stipa tenacissima</i>	<i>Thymus hyemalis</i> , <i>Chamaerops humilis</i> L., <i>Brachypodium retusum</i> (Pers.) P. Beauv., <i>Ulex parviflorus</i>

evaluated (DOY 170 to 315). No gap filling has been performed. Gaps in flux data are present notably in late July to early August (Fig. 2).

2.2. Mediterranean grassland site

Balsa Blanca site is a tussock grassland steppe dominated by *Stipa tenacissima* L. (91% cover) located within the “Cabo de Gata-Níjar Natural Park” (Spain) the only subdesertic protected region in Europe, with a semiarid Mediterranean climate. Annual rainfall is highly variable from year to year with mean values of 375 mm and mean annual temperature of 18.1 °C. In the closer long-term station the average was 200 mm (records from the closest meteorological station, Níjar, distant 30 km) (Rey et al., 2012) with rainfall falling mostly in fall and winter and a prolonged summer drought. The fraction of vegetation cover is 60%, with mean average height of 0.7 m. The soil is classified as Mollic Leptosol (WRB) (*World Reference Base for Soil Resources*, FAO 1998) with depth ranging from 15 to 25 cm.

In situ data were acquired during the 2011 growing season between January and June. This period should capture most of the annual variability in λE although it is only part of a complete growing season that starts in fall until early summer (Fig. 2). Latent and sensible heat fluxes were measured with respective Eddy Covariance (EC) systems using a three-dimensional sonic anemometer (CSAT-3 Campbell Scientific Ltd) and an IRGA (open-path infrared gas analyzer, Li-Cor, Li-7500, Campbell Scientific Ltd). The measurement heights were 3.5 m. Sensors measured at 10 Hz and fluxes were estimated and stored half-hourly applying the corrections for axis-rotation (Kowalski et al., 1997; Mcmillen, 1988) and density fluctuations (Webb et al., 1980).

Net radiation was obtained using NR-Lite (Kipp&Zonen). Four soil heat flux plates (HFP01SC; Campbell Sci. Inc.) were placed at 8 cm depth, two under plant and two under bare soil, and connected via multiplexer to a datalogger. The soil heat flux at the surface was determined by adding the measured heat flux at 8 cm (G) to the energy stored in the layer above the heat plate estimated from soil temperature and soil moisture measurements. Soil temperature was measured using soil thermocouples (TCAV) at 2 and 6 cm depth adjacent to the heat flux plates. Land surface temperature was measured with three Apogee sensors over bare soil, vegetation, and a composite of bare soil and vegetation, (IRTS-P). Air temperature and relative humidity were measured with thermohygrometers (HMP45C, Campbell Scientific Ltd.). Rainfall was measured using a tipping bucket rain gage of 0.25 mm of resolution (ARG100 Campbell Scientific INC., USA). Time domain reflectometry sensors (CampbellCS616, Campbell Scientific Ltd) measured

Volumetric (m^3m^{-3}) soil water content (SWC) under bare soil and under plants with 4 cm being the top most measured soil moisture.

Fig. 2 shows the seasonal dynamics for volumetric soil water content, expressed in % (SWC), rainfall (mm), evapotranspiration (λE) in Wm^{-2} , and NDVI for the two study sites.

2.3. Satellite data

NDVI data were acquired from the Moderate Resolution Imaging Spectroradiometer (MODIS) Terra and Acqua sensor products MOD13Q1 and MY13Q1 (collection 5) over the two study sites. This product consists of 16-day composites of 250 m pixel (Huete et al., 2002). LAI and f_{PAR} products from Terra and Acqua (MOD15A2, MY15A2) consisting of 8-day composites of 1 km pixel (collection 5) (Myneni et al., 2002) were acquired as well. To get daily estimates a linear interpolation using both Terra and Acqua values was performed within the 8-days or 16 day interval in each case.

Land Surface Temperature (LST) and broadband surface albedo (α) products used in this work were developed by the Satellite Application Facility for Land Surface Analysis (LSA SAF) with data from the Spinning Enhanced Visible and Infrared Imager (SEVIRI) radiometer, onboard of the MSG (Meteosat Second Generation). The MSG-SEVIRI sensor includes 12 separate channels and 15 min temporal resolution making it attractive for applications requiring intra-daily information. As for any geostationary satellite the trade-off is the low spatial resolution of 4.8 km at nadir (spatial sampling is 3 km) and large view angles (Schmetz et al., 2002). The LST algorithm is based on a generalized split window, following (Wan & Dozier, 1996) formulation adapted to SEVIRI data (Trigo et al., 2008). It requires information on clear-sky conditions and TOA brightness temperatures for the split-window channels 10.8 mm and 12.0 mm. Channel and broadband emissivity are estimated as a weighted average of that of bare ground and vegetation elements within each pixel using the fraction of vegetation cover derived from NDVI (Trigo et al., 2008). The albedo product is based on shortwave channels at 0.6, 0.8 and 1.6 μm . It has an effective temporal scale of 5 days and updated on a daily basis using cloud-free reflectance observations that are corrected for atmospheric effects using the simplified radiative transfer code SMAC (Geiger et al., 2008). Dynamic information on the atmospheric pressure and total column water vapor comes from the European Centre for Medium-range Weather Forecasts (ECMWF) NWP model. Cloud identification and cloud type classification are used in the processing of all LSA SAF products.

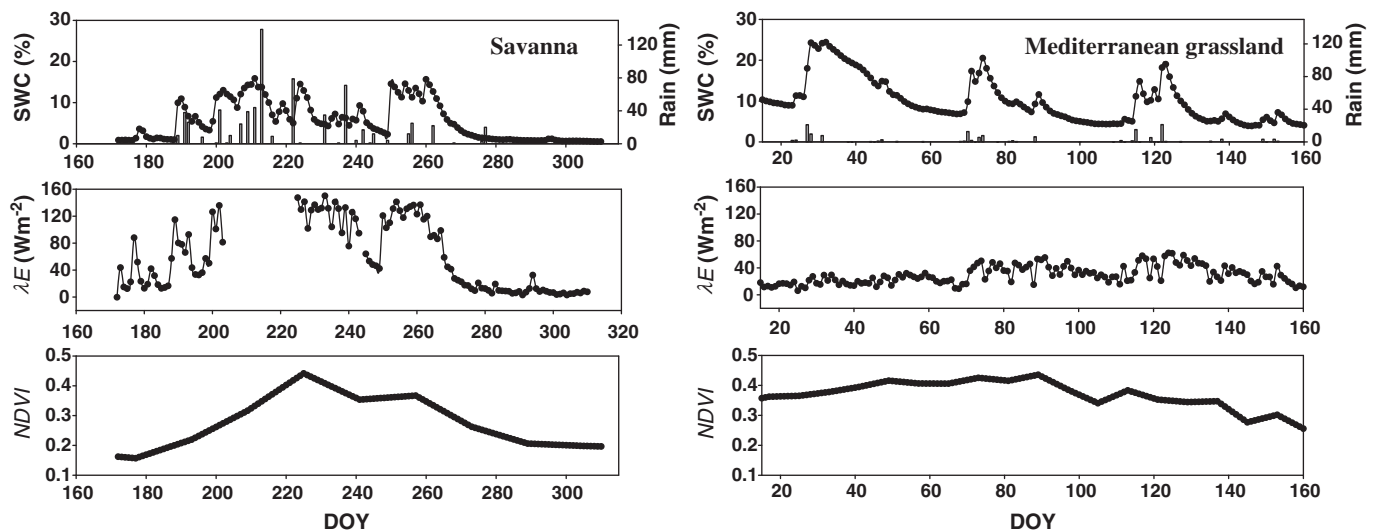


Fig. 2. Volumetric soil water content % (SWC), rainfall (mm), evapotranspiration (λE) in Wm^{-2} , and NDVI dynamics during the periods of analyses in the Sahelian savanna (Agoufou) in 2007 and in the Mediterranean grasslands (Balsa Blanca) in 2011. SWC probes were located at 5 cm and 4 cm depth respectively.

3. Methods

3.1. PT-JPL-daily model description

The daily model proposed here (hereafter PT-JPL-daily) is a modified version of the algorithm described in Fisher et al. (2008) where “ λE ” is partitioned into canopy transpiration (λE_c) and soil evaporation (λE_s) (Eq. 1). In this paper, we did not consider interception evaporation (λE_i), or evaporation from a wet canopy surface, as in low LAI ecosystems it accounts for a limited amount of the total water flux (Mu et al., 2011) and in turn using it requires observations of relative humidity at the sites. However, preliminary model evaluations showed that including it did not improve or worsen the results.

Actual λE is calculated based on potential evapotranspiration of soil (λE_{p_s}) and canopy (λE_{p_c}) which are reduced from their potential level using different constraints (multipliers) based on plant physiological status and soil moisture availability (Fisher et al., 2008). λE_p was calculated using Priestley and Taylor (1972) equation.

$$\lambda E = \lambda E_c + \lambda E_s. \quad (1)$$

Three plant physiological constraints were considered to regulate evapotranspiration: green canopy fraction, a plant temperature constraint (f_T) and a plant moisture constraint (f_M) (Eq. 2).

$$\lambda E_c = f_g f_T f_M \lambda E_{p_c}. \quad (2)$$

All the equations and variables are described in Table 2. Considering that the physiological capacity for energy acquisition should be adjusted with the capacity for transpiration, the green canopy fraction, that represents the canopy fraction actively transpiring, should reflect an upper limit for transpiration. f_g was estimated as the ratio between intercepted and absorbed photosynthetically active radiation f_{APAR}/f_{IPAR} (Table 2). The original model formulation for estimating LAI and f_{APAR} using NDVI and the extinction of radiation equation (see Table 2) was used as well as new estimates of LAI and f_{APAR} derived from MODIS standard products.

The plant temperature constraint (f_T) accounts for reductions in photosynthetic efficiency when plants grow at temperatures departing from their optimum temperature range (Potter et al., 1993). f_T depends on the optimum air temperature for plant growth T_{opt} (°C) and T_{am} (°C) the average daily temperature. In the original model, T_{opt} was assumed to coincide with maximum canopy activity and was estimated as the air temperature of the month with the highest NDVI and radiation and minimum vapor pressure deficit (VPD) (June et al., 2004). However, this approach in Mediterranean semi-arid environments is prone to unrealistic T_{opt} values due to the decoupling between warm and rainy seasons, with the maximum peak for vegetation activity occurring in late winter (García et al., in review). In a preliminary evaluation we observed that the f_T from the Carnegie–Ames–Stanford Approach model (CASA) performed better. In the CASA model f_T has an asymmetric bell shape reflecting a higher sensitivity to high than to low temperatures (see Table 2 for equations) (Potter et al., 1993). To avoid calibrations of T_{opt} depending on the site, we fixed T_{opt} in 25 °C, a value that has been applied in global modeling studies across different types of biomes (Yuan et al., 2010). We checked in preliminary analyses that variations of ± 5 °C around this value of T_{opt} did not affect model outputs.

The third constraint for λE_c was a plant moisture constraint, f_M , defined as the relative change in light absorbance with respect to the maximum ($f_{APAR}/f_{APARmax}$). This approach assumes that plant absorbance decreases mostly due to moisture stress (Fisher et al., 2008).

The soil evaporation component was constrained by a soil moisture limitation, f_{SM} (Eq. 3).

$$\lambda E_s = f_{SM} \lambda E_{p_s}. \quad (3)$$

In this work, we evaluated an f_{SM} estimate based on the thermal inertia (TI) concept using T_s and albedo. Thermal inertia is a physical property of soil at the land surface measuring the thermal response of a material to the changes in its temperature (Nearing et al., 2012). The higher the TI the lower its diurnal temperature fluctuation. Estimating

Table 2

Equations and variables involved in estimating PT-JPL-daily model biophysical constraints, plant variables and energy variables. f_{APAR} is the fraction of Absorbed Photosynthetically Active Radiation, f_{IPAR} the fraction of intercepted photosynthetically active radiation, T_{opt} is optimum temperature for plant growth (25 °C), T_{am} (daily mean air temperature, °C), $f_{APARmax}$ is maximum f_{APAR} , SWC, Soil Water Content ($m^3 m^{-3}$), RH is relative humidity (%), VPD is the vapor pressure deficit (kPa), ATI is the observed apparent thermal inertia index ($^{\circ}C^{-1}$), ATI_{min} is the seasonal minimum ATI, ATI_{max} is the seasonal maximum ATI. Rn is daily net radiation (Wm^{-2}). Values for parameters: $k_{RH} = 0.6$ (Impens & Lemeur, 1969); $k_{PAR} = 0.5$ (Brownsey et al., 1976); $m_1 = 1.16$; $b_1 = -0.14$; (Myneni & Williams, 1994); $m_2 = 1.0$; $b_2 = -0.05$ (Fisher et al., 2008), γ (psychrometric constant) = 0.066 kPa C^{-1} ; $\beta = 1$ kPa, $\alpha_{PT} = 1.26$ Priestley–Taylor coefficient; Δ is the slope of the saturation-to-vapor pressure curve ($Pa K^{-1}$). In the reference column it has been added original model for the cases when the formulation was used in Fisher et al. (2008) or this study if the formulation has been implemented in this study.

	Variable	Description	Equation	Reference
Biophysical constraints	f_g	Green canopy fraction	$f_g = \frac{f_{APAR}}{f_{IPAR}}$	Fisher et al. (2008) original model
	f_T	Plant temperature constraint	$f_T = 1.1814 \cdot \left[1 + e^{0.2 \cdot (T_{opt} - 10 - T_{am})} \right]^{-1}$	Potter et al. (1993) this study
	f_M	Plant moisture constraint	$f_M = \frac{f_{APAR}}{f_{APARmax}}$	Fisher et al. (2008) original model
	f_{SM}	Soil moisture constraint	<ul style="list-style-type: none"> • $f_{SM-SWC} = 1 - \left(\frac{SWC - SWC_{min}}{SWC_{max} - SWC_{min}} \right)$ • $f_{SM-Fisher} = RH^{VPD/\beta}$ • $f_{SM-ATI} = \left(\frac{ATI - ATI_{min}}{ATI_{max} - ATI_{min}} \right)$ 	Fisher et al. (2008) original model Fisher et al. (2008) original model Verstraeten et al. (2006b) this study
Plant variables	f_{APAR}	PAR fraction absorbed by green vegetation	<ul style="list-style-type: none"> • $f_{APAR-NDVI} = m_1 \cdot NDVI + b_1$ • $f_{APAR-MODIS}$ 	Myneni & Williams (1994) original model Myneni et al. (2002) this study
	f_{IPAR}	PAR fraction intercepted by total vegetation	$f_{IPAR} = m_2 \cdot NDVI + b_2$	Fisher et al. (2008) original model
	f_c	fractional vegetation cover	$f_c = f_{IPAR}$	Campbell & Norman (1998) original model
	LAI	Leaf Area Index	<ul style="list-style-type: none"> • $LAI_{NDVI} = -\ln(1 - f_c)/k_{PAR}$ • LAI_{MODIS} 	Norman et al. (1995); Ross (1976) original model Myneni et al. (2002) this study
Energy variables	Rn_s	Net radiation to the soil	$Rn_s = Rn \cdot e^{(-k_{RH} LAI)}$	Norman et al. (1995); Ross (1976) original model
	λE_{p_c}	Priestley–Taylor potential evapotranspiration for canopy	$\lambda E_{p_c} = \alpha_{PT} \frac{\Delta}{\Delta + \gamma} (Rn - Rn_s)$	Norman et al. (1995) original model
	λE_{p_s}	Priestley–Taylor potential evapotranspiration for soil	$\lambda E_{p_s} = \alpha_{PT} \frac{\Delta}{\Delta + \gamma} (Rn_s - G)$	Norman et al. (1995) original model

thermal inertia requires knowing thermal conductivity of the material (K), its density (ρ) and specific heat (C) (Price, 1977).

Increasing soil moisture content modifies soil thermal conductivity and reduces the diurnal surface temperature fluctuation (Verstraeten et al., 2006b). In early studies, this diurnal T_s variation was linked theoretically to thermal inertia resulting in the apparent thermal inertia (ATI) index (Price, 1977). Estimating thermal inertia using remote sensing was first introduced by Price (1977) and expanded by Cracknell and Xue (1996). Sobrino et al. (1998) and Lu et al. (2009). In this study we estimated ATI following Verstraeten et al. (2006b) which was based on Mitra and Majumdar (2004) (see Eq. 4). ATI relies on broadband albedo (α), and the difference between maximum daytime (T_{SDMax}) and minimum nighttime (T_{SDmin}) surface temperature, and a solar correction factor C (Eq. 5) that normalizes for changes in solar irradiance with latitude, ϑ and the solar declination angle φ , the angle between sun rays and the plane of the Earth's equator. It is assumed that ATI reflects both soil and canopy water content if the T_s includes both soil and vegetation components (Tramutoli et al., 2000; Verstraeten et al., 2006b). In fact, a composite T_s might track better changes in root-zone SWC as the canopy temperature responds rapidly to changes in root zone SWC, which can be decoupled from the bare soil surface SWC. From the 15 minute T_s data the minimum (T_{SDmin}) and maximum (T_{SDMax}) values from each day were extracted. Observations flagged as cloudy in the METEOSAT LST data and days when the midday observation was missing were excluded from the analyses. A smoothing procedure averaging with the prior and following day was applied to the ATI assuming that the soil moisture conditions could be interpolated between subsequent days and to remove noise.

$$ATI = C \frac{1 - \alpha}{T_{SDMax} - T_{SDmin}} \quad (4)$$

$$C = \sin \vartheta \sin \varphi \cdot (1 - \tan^2 \vartheta \cdot \tan^2 \varphi) + \cos \vartheta \cdot \cos \varphi \cdot \arccos(-\tan \vartheta \cdot \tan \varphi). \quad (5)$$

Where ϑ is latitude, and φ is solar declination estimated using the method of Iqbal (1983).

However, the coupling between ATI and soil moisture is not straightforward. Thermal inertia could be converted directly to soil moisture provided that soil properties are known (Lu et al., 2009; Minacapilli et al., 2009; Van Doninck et al., 2011). Since those properties only change over geologic time scales, short-term changes in ATI can be linked to changes in soil moisture using time-series (Van Doninck et al., 2011). Verstraeten et al. (2006b) related soil moisture to remotely sensed ATI derived from METEOSAT imagery by assuming that the minimum and maximum seasonal ATI (ATI_{min} and ATI_{Max}) correspond to residual and saturated soil moisture contents obtaining f_{SM-ATI} (see equation in Table 2).

To evaluate f_{SM} derived from ATI two additional formulations of f_{SM} used in the original model formulation have been also tested (see Table 2). The first is based on field measurements of Volumetric soil water content (SWC) (f_{SM-SWC}), where SWC was rescaled between a minimum (SWC_{min}) and a maximum value (SWC_{Max}) (Fisher et al., 2008). In our case, SWC_{min} was estimated as the minimum value of the dry season. SWC_{Max} was estimated as the value of SWC in the 24 h after a strong rainfall event, which can be considered as an estimate of the field capacity. If $SWC > SWC_{Max}$ then $f_{SM-SWC} = 1$. In the Mediterranean site, the 2006–2011 period was used to extract SWC_{min} and SWC_{Max} as the period used to apply PT-JPL-daily was not a complete season.

The second approach to estimate f_{SM} was the original PT-JPL model formulation based on the link between atmospheric water deficit and soil moisture ($f_{SM-Fisher}$) (Bouchet, 1963; Morton, 1983). This link is compromised if the vertical adjacent atmosphere is not in equilibrium with the underlying soil (Fisher et al., 2008). The β parameter indicates the relative sensitivity of soil moisture to VPD (see Table 2).

3.2. Global sensitivity analyses (EFAST) approach

Sensitivity analysis can be used to evaluate the effects of uncertainty on input or parameters on model output or to evaluate which variables or parameters have the largest effect on model output (Matsushita et al., 2004). In this study Global Sensitivity Analysis (GSA) of PT-JPL-daily model was performed using Extended Fourier Amplitude Sensitivity Test (EFAST) (Saltelli et al., 1999). EFAST was originally developed by Cukier et al. (1978) and improved by Saltelli et al. (1999). The advantage of EFAST compared to traditional sensitivity analyses such as one-at-a-time (OAT) or experimental design (ED) is that it allows several input variables to vary simultaneously considering interactions among them. It can be used for non-linear and non-monotonic models providing similar results to more complex methods based as well on analyses of variance but being computationally more efficient (Saltelli et al., 1999). A Fourier decomposition is used to obtain the fractional contribution of the individual input factors to the variance of the model prediction (Campolongo et al., 2000).

To identify the relative importance of each model input in terms of its contribution to the output variance of daily evapotranspiration, perturbations for each variable were applied around the mean value of the growing season and also around mean monthly values. Rn , G , $NDVI$ and T_{air} were varied by $\pm 10\%$ around their monthly means and annual mean based on reported uncertainty of field measurements for those variables (García et al., 2008). For the constant model parameters: m_1 , b_1 , m_2 , b_2 , k_{Rn} , and k_{PAR} , the range of uncertainty was based on values used in the literature (Table 3). A perturbation of $\pm 25\%$ around the mean was considered for the soil moisture constraint (f_{SM}) and the plant temperature constraint (f_T).

3.3. Evaluation of the PT-JPL-daily evapotranspiration model

PT-JPL-daily was run using a combination of field and remotely-sensed data as inputs to parameterize the biophysical constraints and partition the energy between soil and canopy (Table 4). Two versions (the original version and one version using MODIS products) of LAI and f_{APAR} were tested which modify two of the plant constraints f_g , and f_M as well as the energy partition between soil and vegetation (Table 2). In addition, three versions of f_{SM} were used as explained in the model description section (Table 2). Model results were compared with λE from Eddy Covariance fluxes and the coefficient of determination (r^2), Mean Average Error (MAE), the bias, the RMSE (Root Mean Square Error) and MPE (Mean Absolute Percentage Error) were used as indicators of model performance. To compare modeled λE with λE measurements from Eddy Covariance the energy balance from the

Table 3

Ranges of variation for input parameters and variables in PT-JPL-daily model. For Rn , G , $NDVI$ and T_{air} ranges of $\pm 10\%$ around monthly means and annual mean were considered. For the constant model parameters: m_1 , b_1 , m_2 , b_2 , k_{Rn} , and k_{PAR} , the range of uncertainty was based on values used in the literature. For the soil moisture constraint (f_{SM}) and the plant temperature constraint (f_T) a range of $\pm 25\%$ around the mean was considered. Description of variables and parameters can be found in Table 2.

Input var	Range	Reference
T_{air}	$\pm 10\%$ of mean value	This study
Rn	$\pm 10\%$ of mean value	This study
G	$\pm 10\%$ of mean value	This study
f_T	$\pm 25\%$ of mean value	This study
f_{SM}	$\pm 25\%$ of mean value	This study
$NDVI$	$\pm 10\%$ of mean value	This study
m_1	[1.16, 1.42]	This study
b_1	[-0.039, -0.025]	This study
m_2	[0.9, 1.2]	Fisher et al. (2008)
b_2	[-0.06, -0.04]	Fisher et al. (2008)
k_{Rn}	[0.3, 0.6]	Ross (1976)
k_{PAR}	[0.3, 0.6]	Ross (1976)

Table 4

Eight versions of PT-JPL-daily (FD) were run based on different combinations of equations and data used for the variables: f_{SM} , f_{IPAR} and LAI . Rn is Net radiation (Wm^{-2}), G is soil heat flux (Wm^{-2}), T_{air} air temperature ($^{\circ}C$), SWC , Soil Water Content (%), VPD , Vapor pressure deficit (kPa), RH , Relative humidity (%), T_s , Surface temperature ($^{\circ}C$), LAI (Leaf Area Index), f_{PAR} (fraction of Photosynthetic Active Radiation) and α broadband surface albedo. The soil moisture constraints used were: f_{SM-SWC} (from measured volumetric soil water content), $f_{SM-Fisher}$ (from atmospheric water deficit), and f_{SM-ATI} (from apparent thermal inertia). Two different f_{APAR} and LAI were used (a) $f_{APAR-NDVI}$ and LAI_{NDVI} (FDA model versions) and (b) used $f_{APAR-MODIS}$ and LAI_{MODIS} (in FDb model versions). All equations are described in Table 2.

Algorithm version	Algorithm name	f_{SM}		f_{APAR} and LAI		Common variables
		Estimate	Data/source	Estimate	Data/source	Data/source
1	FDa _{SWC}	f_{SM-SWC}	SWC/in situ	$f_{APAR-NDVI}$ LAI_{NDVI}	NDVI/MODIS	Rn , G , T_{air} /in situ NDVI/MODIS
2	FDb _{SWC}			$f_{APAR-MODIS}$ LAI_{MODIS}	f_{PAR} , LAI/MODIS	
3	FDa _{Fisher}	$f_{SM-Fisher}$	VPD, RH/in situ	$f_{APAR-NDVI}$ LAI_{NDVI}	NDVI/MODIS	
4	FDb _{Fisher}			$f_{APAR-MODIS}$ LAI_{MODIS}	f_{PAR} , LAI/MODIS	
5	FDa _{ATI-in situ}	f_{SM-ATI}	T_s , α /in situ	$f_{APAR-NDVI}$ LAI_{NDVI}	NDVI/MODIS	
6	FDb _{ATI-in situ}			$f_{APAR-MODIS}$ LAI_{MODIS}	f_{PAR} , LAI/MODIS	
7	FDa _{ATI-MSG}		T_s , α /MSG	$f_{APAR-NDVI}$ LAI_{NDVI}	NDVI/MODIS	
8	FDb _{ATI-MSG}			$f_{APAR-MODIS}$ LAI_{MODIS}	f_{PAR} , LAI/MODIS	

Eddy Covariance data should be forced to zero (Twine et al., 2000). We used the criteria of preserving the Bowen ratio that assumes that the Bowen ratio ($H/\lambda E$) is well measured by the EC system and the closure error is proportionally distributed into λE and H (Twine et al., 2000).

The evaluation results (r^2 , errors and biases) are presented in four steps. First, model performance using measured soil moisture constraint (f_{SM-SWC}) was analyzed. Here, the accuracy of the two different versions for LAI and f_{APAR} was compared as, in principle, this model version using f_{SM-SWC} should be the most precise from the point of view of soil moisture constraint and can be used as a benchmark. In the second step, the feasibility of using $f_{SM-Fisher}$, from atmospheric variables at daily time-scale in semiarid conditions was evaluated. In the third step, the performance of the model run with the apparent thermal inertia index f_{SM-ATI} from in-situ and also satellite data was evaluated. In this three steps the two versions for estimating LAI and f_{APAR} were evaluated as well resulting in a total of eight algorithm versions evaluated (see Table 4). Finally, to place model results in the context of global drylands, our accuracy results were compared to published accuracy results from other models that used remote sensing information at the same and at other dryland savanna and grasslands sites across the globe. In those cases when model outputs were provided by the authors at 30 minutes time step, they were aggregated at daily time scale and compared with the Eddy Covariance data to have comparable statistics.

4. Results and discussion

4.1. Global sensitivity analyses (EFAST) approach

Considering the variability around mean annual conditions, the contribution to uncertainty was less than 20% for most parameters and variables in the Sahelian savanna. The greatest uncertainty was due to two of the biophysical constraints: f_{SM} and f_T with 22.19% and 17.68% respectively (total effect). Five other variables involved in LAI estimation and energy partition between soil and canopy contributed around 12% to model uncertainty (Fig. 3). However, the relative importance of each variable depends on the time of the year. At the beginning of the season, λE was most sensitive to accuracy in f_{SM} reaching the maximum value of explained variance among all variables and months (40%). During the maximum peak of $NDVI$, in the middle of the season, the greatest sensitivity was due to f_T , and m_1 (involved in

f_M and f_g estimates via f_{APAR}). During the senescent phase, the model was more sensitive to accuracy in k_{PAR} and k_{Rn} , involved in energy partition into soil and vegetation.

Under annual Mediterranean conditions, most of the uncertainty was related to the partition of energy between soil and vegetation, shown by the highest sensitivity to the two coefficients of extinction of radiation: k_{PAR} (50%) involved in LAI estimates, and k_{Rn} (20%) both contributing to estimate the net radiation reaching the soil component. This is similar to the situation during the senescent phase in the Sahel. Seasonally, the relative importance of each variable was similar to the annual pattern, except in January when modeled λE was more sensitive to accuracy in Rn .

Fig. 3 shows how in both ecosystem types, mean effect and total effect (that considers interactions) on evapotranspiration were very similar with differences around 1–2%, indicating low effect of variable interactions.

4.2. Evaluation of the PT-JPL-daily evapotranspiration model with Eddy Covariance data

4.2.1. Soil moisture constraint from measured soil moisture (f_{SM-SWC})

In the Sahelian savanna the performance of PT-JPL-daily λE model using measured SWC (f_{SM-SWC}) was similar regardless of the f_{APAR} and LAI estimate used (FDa_{SWC} or FDb_{SWC}) ($r^2=0.85-0.86$ and $MAE=14.14-13.54$) (Table 5 and Fig. 4a, b). In the Mediterranean grasslands, both the coefficient of determination and errors were also similar regardless of the f_{APAR} and LAI used ($r^2=0.75-0.74$; $MAE=10.66-11.44$) (Table 5 and Fig. 5a, b). Therefore, PT-JPL-daily formulation is capable to reproduce the dynamics of λE in the Mediterranean grasslands, as it explained 75% of the λE variance. Considering that the uncertainty of the energy balance closure from Eddy Covariance data in this Mediterranean site, calculated at daily time scale, represents 21.7% of the available energy ($Rn-G$), the accuracy obtained with PT-JPL-daily using f_{SM-SWC} is closest to the one from Eddy Covariance. In the Sahel, the model explains up to 86% of the variance, which considering that the closure error is 5.78% of the available energy at daily scale is also close to the instrumental accuracy. However, in this site during the growing season there was a systematic underestimate of λE during the period of maximum growth followed by an overestimate, independently of the f_{APAR} and LAI used (Fig. 4a and b).

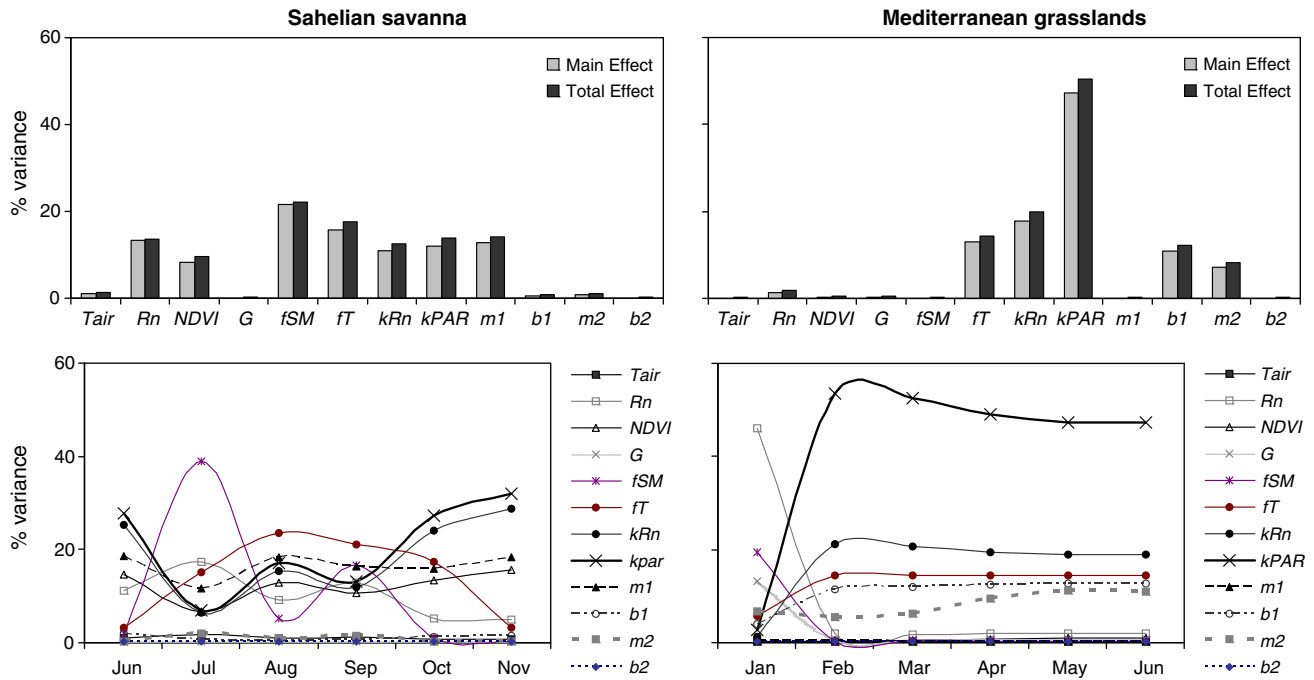


Fig. 3. Upper panels: sensitivity of modeled evapotranspiration according to mean annual conditions (% percentage of explained variance). Main effect is the variance explained without considering interactions among variables and total effect considering interactions. Lower panels: sensitivity of modeled evapotranspiration considering monthly conditions in the Sahelian savanna and Mediterranean grasslands (total effect). Uncertainty levels were set as $\pm 10\%$ of the mean for input variables NDVI, T_{air} , R_n , and G and of $\pm 25\%$ of the mean for the soil moisture (f_{SM}) and plant temperature (f_T) constraints. For constant model parameters: m_1 , b_1 , m_2 , b_2 , k_{Rn} , and k_{PAR} , the range of uncertainty was based on values used in the literature.

To assess whether this mismatch in the Sahelian site could be related to the LAI and f_{PAR} estimates, we compared satellite LAI estimates with field estimates and also evaluated the evapotranspiration model ran with field estimates for LAI and f_{PAR} . Comparison of LAI satellite products with field estimates (Fig. 6a) showed better correlations with MODIS

LAI ($r^2 = 0.93$) than for LAI estimated from $NDVI$ ($r^2 = 0.71$). Although MODIS LAI underestimated the maximum peak and overestimated LAI during growing and senescence stages its phenology pattern matched better with the field data than the LAI derived from $NDVI$ (Fig. 6a). In this case, the maximum LAI happened earlier in the season than the field maximum LAI , showing also greater overestimates during growing and senescent phases. This could explain a slightly better performance of the λE model using MODIS products during the growing season (Table 6).

Table 5

Evaluation of PT-JPL-daily λE with Eddy Covariance data. In the savanna the results have been evaluated between June and December 2007 and in the Mediterranean grasslands between January and June 2011. Model versions starting with “FDa” were run with $f_{APAR-NDVI}$ and LAI_{NDVI} and with “FDb” with $f_{APAR-MODIS}$ and LAI_{MODIS} . f_{SM-SWC} is the soil moisture constraint derived from measured volumetric soil water content, and f_{SM-ATI} from apparent thermal inertia. Surface temperature and albedo could be acquired from in-situ sensors or from satellite (MSG) sensors.

Site	f_{SM}	Model version	r^2	MAE ^a	Bias ^b	RMSE ^c	MAPD (%) ^d
Sahelian savanna (all dates)	In-situ	FDa _{SWC}	0.85	14.14	7.59	21.45	22.69
		FDb _{SWC}	0.86	13.54	4.02	20.39	21.72
		FDa _{ATI-in situ}	0.82	20.69	-1.48	23.88	33.20
	Satellite	FDb _{ATI-in situ}	0.83	19.72	-7.14	23.10	31.65
		FDa _{ATI-MSG}	0.79	23.11	16.52	30.55	37.09
		FDb _{ATI-MSG}	0.80	20.21	11.78	26.53	32.43
Mediterranean grasslands (growing season)	In-situ	FDa _{SWC}	0.75	10.66	10.10	12.43	30.89
		FDb _{SWC}	0.74	11.44	10.96	13.2	33.16
		FDa _{ATI-in situ}	0.58	9.66	5.70	11.10	28.01
	Satellite	FDb _{ATI-in situ}	0.57	9.85	6.21	11.58	28.57
		FDa _{ATI-MSG}	0.32	10.16	-3.01	14.48	29.46
		FDb _{ATI-MSG}	0.31	10.78	-3.80	15.03	31.26

^a Mean absolute difference $MAE = (\sum_{i=1}^n |O_i - P_i| / n)$.
^b Bias $bias = (\sum_{i=1}^n (O_i - P_i)) / n$.
^c Root mean square error $RMSE = [(\sum_{i=1}^n (O_i - P_i)^2 / n)]^{1/2}$.
^d Mean absolute percentage difference $MAPE = \frac{100}{<O>} (\sum_{i=1}^n |O_i - P_i| / n)$, where P_i is the model-predicted value, O_i is the observed value, $<O>$ is the mean observed value, n is the number of observations.

However, model outputs ran using field measured LAI , fc and f_{APAR} (estimated as described in Mougin et al., 2009) did not improve model performance (see Table 6). Therefore, using satellite products for vegetation (LAI and f_{PAR}) to run the model produce similar results than using field vegetation estimates.

It seems that when vegetation is changing very rapidly around the seasonal peak in the Sahel, the model can account for the general pattern of λE but not for minor ups and downs observed in the Eddy Covariance λE . Increasing the energy partition allocated to vegetation by using k_{Rn} of 0.75, a value obtained by optimization at the site (Ridler et al., 2012), improved significantly the results ($r^2 = 0.76$ vs $r^2 = 0.68$) (Table 6). Using this coefficient reduced the λE offset after the LAI peak, but not before (Fig. 6b). It should be noted that field LAI estimates (Fig. 7) present uncertainty as well, as they were interpolated between the field samplings, acquired every ≈ 10 days. Thus, before the maximum LAI peak (DOY = 235) the previous field sampling was 10 days earlier, making it possible to miss a higher and earlier maximum peak. In that case, LAI underestimates would produce λE underestimates between the periods DOY225 and DOY235 (Fig. 6).

These results suggest that the model could benefit from an improved energy partitioning between soil and canopy considering variable extinction coefficients and separate longwave and shortwave components (Kustas & Norman, 1999), as well as from shorter-time scale estimates of LAI and f_{PAR} .

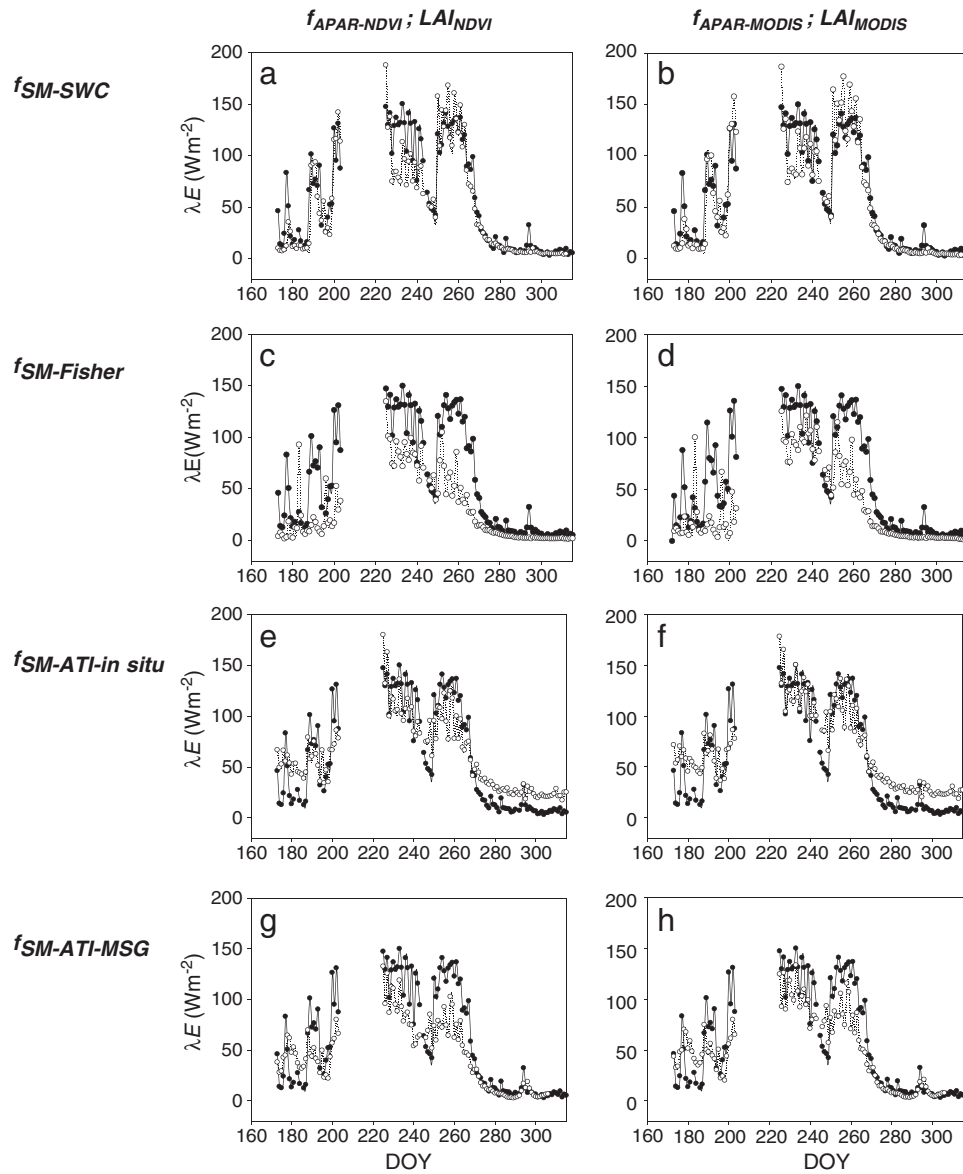


Fig. 4. Daily λE (Wm^{-2}) in the Sahelian savanna (Agoufou, Mali) from Eddy Covariance data (black dots) and modeled (white dots) during 2007. In the first column (figures a, c, e, g) the model was run using $f_{APAR-NDVI}$ and LAI_{NDVI} and in the second column (figures b, d, f, h) using $f_{APAR-MODIS}$ and LAI_{MODIS} . In each of the six rows, the model was run a different soil moisture constraint: f_{SM-SWC} from measured volumetric soil water content (figures a, b), $f_{SM-Fisher}$ from atmospheric water deficit (figures c, d), $f_{SM-ATI-in\ situ}$ from apparent thermal inertia from in-situ measurements (figures e, f), $f_{SM-ATI-MSG}$ from apparent thermal inertia from MSG–SEVIRI measurements (figures g, h).

4.2.2. Soil moisture constraint from atmospheric variables ($f_{SM-Fisher}$)

Estimating λE using $f_{SM-Fisher}$ with the same parameterization as in Fisher et al. (2008) ($\beta = 1$; midday conditions) did not provide meaningful results in the Mediterranean grasslands ($r^2 \sim 0.16$) (Table 7). In the savanna, correlations were better but well below those found for f_{SM-SWC} ($r^2 = 0.61\text{--}0.62$) and with high biases around $25\text{--}29 \text{ Wm}^{-2}$ (Table 4, Figs. 5 and 6). This constraint diagnosed the major water stress during the growing season around DOYs 240–250. We evaluated the sensitivity of $f_{SM-Fisher}$ to β values between 0.05 and 2, and to the use of daily average or midday conditions for RH and VPD . Table 7 shows the results when the model was run with two different values of β . They are shown in the table as they provided the best results in each site: $\beta = 0.1 \text{ kPa}$, that was applied at a global scale in Mu et al. (2007), and $\beta = 1 \text{ kPa}$ applied in Fisher et al. (2008).

In the savanna, the best results corresponded to $\beta = 1 \text{ kPa}$ and daily average conditions ($r^2 = 0.80$; $MAE = 18.08 \text{ Wm}^{-2}$). In the Mediterranean grasslands PT-JPL-daily performed better using $\beta = 0.1$ (Table 7), especially for midday conditions ($r^2 = 0.64\text{--}0.53$) although

λE was systematically underestimated (biases $\approx 15\text{--}17 \text{ Wm}^{-2}$). These results suggest a stronger control of atmospheric conditions on soil moisture changes in the Mediterranean conditions than in the Sahel. Therefore, parameterization using $f_{SM-Fisher}$ should be tuned according to the conditions in each site for successful results.

4.2.3. Soil moisture constraint from apparent thermal inertia (f_{SM-ATI})

Using in-situ data, model performance in the savanna for the thermal inertia index f_{SM-ATI} was practically equivalent to that using SWC (f_{SM-SWC}), with $r^2 \approx 0.82$ and slightly higher errors but similar or lower biases (Table 5). Non significant differences were found when using f_{APAR} and LAI from MODIS or a linear function of $NDVI$ except from a slightly lower bias with the latter. At the end of the rainy season (DOY 270), f_{SM-ATI} overestimated λE as even at an entirely dry soil the ATI index will never become zero, since that would require an infinite temperature amplitude (Van Doninck et al., 2011).

In the Mediterranean grasslands, statistics from model performance using f_{SM-ATI} from in-situ data were again not as good as than in the

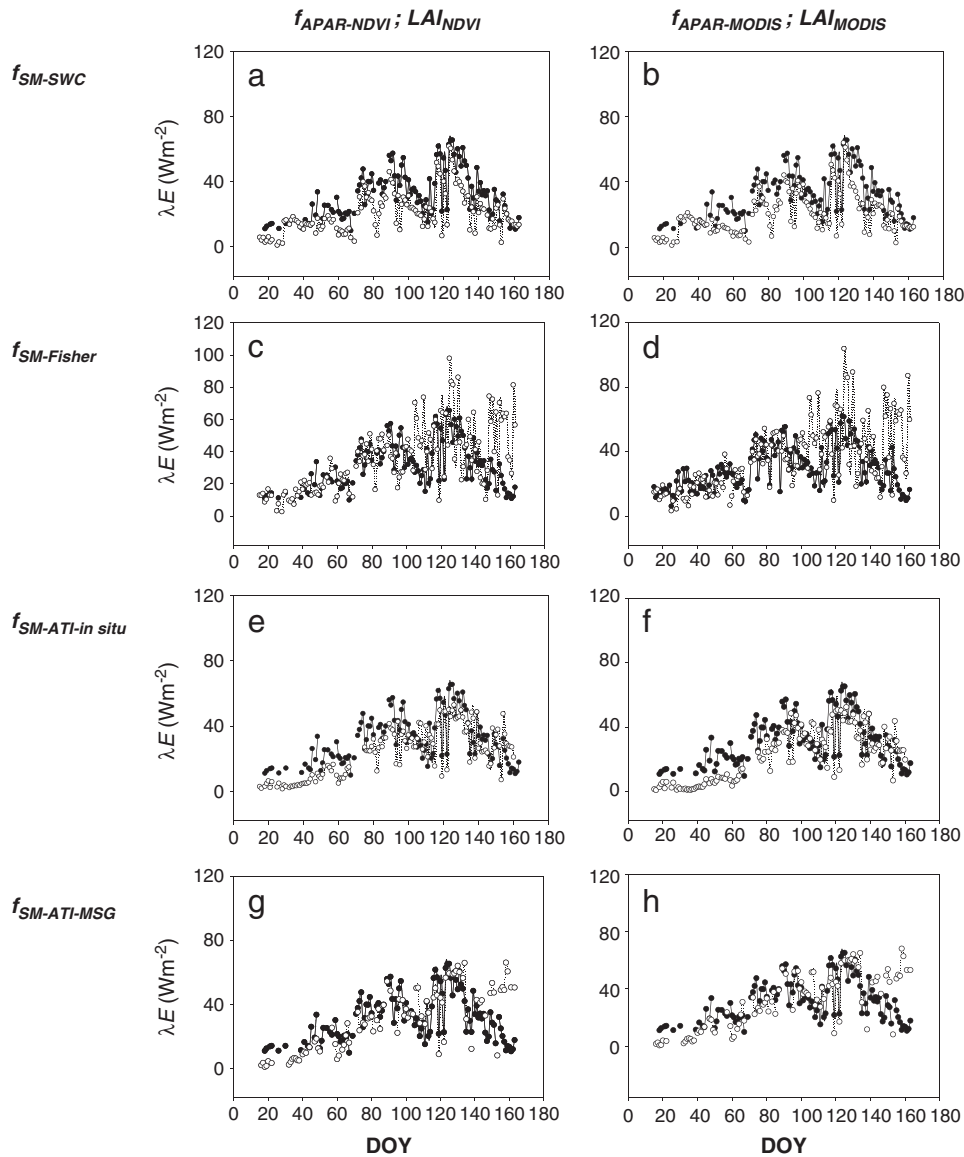


Fig. 5. Daily λE (Wm^{-2}) in the Mediterranean grassland (Balsa Blanca, Spain) from Eddy Covariance data (black dots) and modeled (white dots) during 2007. In the first column (figures a, c, e, g) the model was run using $f_{APAR-NDVI}$ and LAI_{NDVI} and in the second column (figures b, d, f, h) using $f_{APAR-MODIS}$ and LAI_{MODIS} . In each of the six rows, the model was run a different soil moisture constraint: f_{SM-SWC} from measured volumetric soil water content (figures a, b), $f_{SM-Fisher}$ from atmospheric water deficit (figures c, d), $f_{SM-ATI-in\ situ}$ from apparent thermal inertia from in-situ measurements (figures e, f), $f_{SM-ATI-MSG}$ from apparent thermal inertia from MSG-SEVIRI measurements (figures g, h).

savanna. Although the r^2 using f_{SM-ATI} was lower than those obtained with f_{SM-SWC} , the errors decreased and the biases were half of those obtained with f_{SM-SWC} . Similar to the savanna site, results were quite similar independently of the LAI and f_{PAR} estimate used to run the model.

When running the model using satellite MSG instead of in-situ data for f_{SM-ATI} , good results were obtained in the savanna site in terms of $r^2 \sim 0.80$ and $MAE = 23.1\text{--}20.1 \text{ Wm}^{-2}$ (Table 5) but higher biases were detected due to λE underestimates during the growing season (Fig. 4g, h). This was due to the fact that the diurnal T_s difference ($T_{sDmax} - T_{sDmin}$) was always higher for MSG than for in-situ data (Fig. 7), producing lower soil moisture (f_{SM}) values.

In the Mediterranean grasslands, using MSG data instead of in-situ to estimate f_{SM-ATI} produced a greater loss of accuracy in r^2 than in the savanna although errors were similar and biases even lower than with in-situ data (Table 5). On one hand, results using in-situ data were worse to start with than in the savanna with correlations around $r^2 = 0.58$. As in the Mediterranean site λE is lower (Fig. 2) the model is less tolerant to different error sources. Besides the noise apparent in the MSG time-series, the comparability of the diurnal temperature

difference ($T_{sDmax} - T_{sDmin}$) between in situ and MSG data was more problematic than in the savanna, with systematically higher MSG values (Fig. 7). Additional inspection of T_s (15 min) observations between field and satellite (Fig. 8) showed that differences between in-situ and satellite were larger in the grasslands ($MAE = 2.43 \text{ }^\circ\text{C}$) than in the savanna ($MAE = 1.56 \text{ }^\circ\text{C}$). In the Mediterranean site the sensor viewing angle is 42.68° while in the Sahel it is only 18.01° . This results in a larger scale mismatch at the Mediterranean site between the satellite pixel and the footprint of the in-situ sensors as well as greater atmospheric effects due to a larger atmospheric path radiance.

The f_{SM-ATI} approach is very sensitive to uncertainty in thermal data since day and night T_s are used in the denominator (Cai et al., 2007; Sobrino et al., 1998; Verstraeten et al., 2006b). Sensitivity to errors is greater when R_n is higher which occurs at the end of the study period in the Mediterranean site and the middle of the season in the Sahelian site (Guichard et al., 2009) (see Figs. 4g, h and 5g, h). In fact, in the Mediterranean grasslands, the lack of fit for f_{SM-ATI} MSG ($r^2 = 0.32\text{--}0.31$) was caused by the last 10 days of the study period (see Fig. 5g and h). Another important limitation of the ATI methodology is the vulnerability

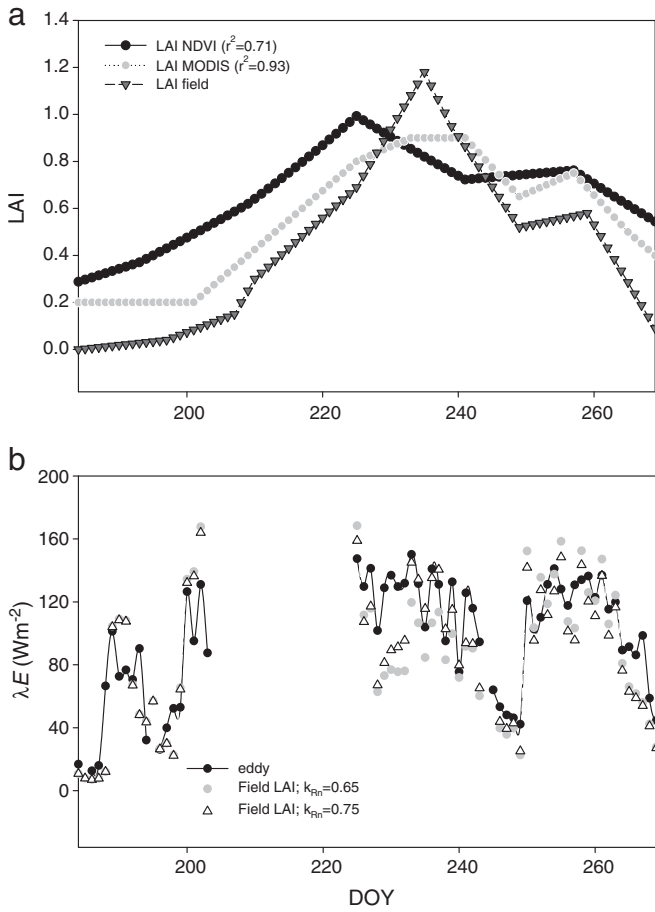


Fig. 6. a) Comparison of LAI estimated from NDVI (LAI_{NDVI}), LAI from MODIS, and LAI from field estimates during the growing season of 2007 in the Sahelian savanna. b) Daily λE (Wm^{-2}) from Eddy Covariance data (black dots) and modeled using LAI from field estimates and $k_{Rn} = 0.65$ (gray dots) and $k_{Rn} = 0.75$ (Triangles). r^2 refers to the coefficient of determination comparing with LAI from field estimates.

to noise introduced by meteorological conditions (Van Doninck et al., 2011). Although we have compared only dates without clouds according to LSA SAF Quality Flags, inspection of SEVIRI images revealed a large cumulus cloud affecting the adjacent pixel of the Mediterranean grasslands location unreported in the Quality Flags during the last 10 days of the period. When excluding those days r^2 increased to 0.64–0.66.

4.3. Comparison with other evapotranspiration models in global dryland ecosystems

In the Sahelian savanna site, a Soil–Vegetation–Atmosphere Transfer (SVAT) model forced with some of the same in-situ climatic

Table 6
Comparison of model performance during the period of field sampling (DOY: 184–269) in the Sahelian savanna (Agoufou). Note that the period used is slightly shorter than for Table 4, and explains why the model statistics for FDa_{SWC} and FDb_{SWC} differ slightly from Model 4 statistics.

f_{APAR} , LAI	Model version	r^2	MAE ^a	Bias ^b	RMSE ^c
$f_{APAR-NDVI}$, LAI_{NDVI}	FDa_{SWC}	0.67	20.53	9.50	26.29
$f_{APAR-MODIS}$, LAI_{MODIS}	FDb_{SWC}	0.69	19.66	3.13	24.97
$f_{APAR-field}$, LAI_{field}	$FD_{field-SWC}$ ($k_{Rn} = 0.60$)	0.68	21.39	11.26	26.10
$f_{APAR-field}$, LAI_{field}	$FD_{field-SWC}$ ($k_{Rn} = 0.75$)	0.76	19.23	9.31	20.96

^a Mean absolute difference $MAE = (\sum_{i=1}^n |O_i - P_i|) / n$.
^b Bias $bias = (\sum_{i=1}^n (O_i - P_i)) / n$.
^c Root mean square error $RMSE = [(\sum_{i=1}^n (O_i - P_i)^2) / n]^{1/2}$ where P_i is the model-predicted value, O_i is the observed value, $<O>$ is the mean observed value, n is the number of observations.

inputs and vegetation parameters was calibrated using multi-objective functions during the 2007 growing season (Ridler et al., 2012).

Calibration of the SVAT model with in-situ T_s and SWC showed better results ($r^2 = 0.81$) (Table 8) than PT-JPL-daily during the growing season calibrated with field data when correlations were around $r^2 = 0.67–0.65$ (see Table 6). Nonetheless, daily errors were similar in magnitude and in fact underestimates were higher (bias = $12.26 Wm^{-2}$, not shown) than with PT-JPL-daily (Table 6). These results are reasonable as the SVAT model, based on the two-source Shuttleworth and Wallace (1985) model coupled to a hydrological model, has a stronger physical basis (Overgaard, 2005). It requires several plant and soil parameters such as root depth, minimum stomatal conductance, soil hydraulic conductivity, as well as atmospheric variables including rainfall, wind speed, and relative humidity at 15-minute time scale. However, calibration of the SVAT model with both MSG and AMSR-E (Advanced Microwave Scanning Radiometer) satellite data for operational purposes decreased correlations to $r^2 = 0.63$ equivalent to PT-JPL-daily results during the growing season (Tables 8 and 6). Results from a simpler modeling approach based on the triangle relationship (Stisen et al., 2008), estimated λE in the Sahel in a site with higher rainfall (487 mm in 2005) with similar error levels to our Agoufou site and also underestimates: $RMSE = 31.00 Wm^{-2}$. Correlations were higher ($r^2 = 0.75$) than in our model. Sun et al. (2011) model results based on a water-deficit index in an open savanna in Sudan using a combination of MODIS and SEVIRI products, produced similar results than PT-JPL-daily run with satellite products ($r^2 = 0.73$ and $MAE = 26 Wm^{-2}$) considering the fact that they acquired T_{air} from ECMWF weather forecast product and we used in-situ T_{air} . In this case, the peak λE was also underestimated. Although the model captures λE changes at the beginning of the season, it seems that the transpiration processes in conditions of the Sahel are difficult to reproduce during the period of plant growth as different studies underestimate λE during the growing season independently of model complexity (Ridler et al., 2012). For instance, in the semiarid savanna in Niger, the SVAT model *SEt_HyS-savanna* that presents an additional tree-layer, systematically underestimated peak λE despite of added model complexity and a high degree of parameterization (Saux-Picart et al., 2009) ($r^2 = 0.66–0.64$, their results have not included in Table 7 as they represent 30 min and not daily estimates).

Compared to other models using remote sensing information in the same Mediterranean grasslands site, PT-JPL-daily performed better. For instance, λE estimates using f_{SM-SWC} were more accurate ($r^2 = 0.75$; $MAE \sim 10 Wm^{-2}$) than those from a Penman–Monteith model adapted by Leuning et al. (2008) (hereinafter PML). In the PML the soil evaporation fraction was estimated with measured SWC , similarly to f_{SM-SWC} (Morillas et al., 2011, in review-a) (Table 8). In addition, the PML required optimization with field-measured λE and meteorological variables such as VPD , or estimation of aerodynamic and surface conductances. Two more operational parameterizations of PML for the soil evaporation fraction based on measured rainfall produced also poorer results for PML at the same site (Table 8) (Morillas et al., 2011, in review), with similar results to PT-JPL-daily run with satellite MSG data for f_{SM-ATI} and poorer than PT-JPL-daily run with f_{SM-ATI} in-situ ($r^2 \approx 0.58$, $MAE \approx 10 Wm^{-2}$).

PT-JPL-daily λE estimates using MSG data for f_{SM} provided also better correlations than a triangle approach run with MODIS T_s and $NDVI$ ($r^2 = 0.24$) despite of lower errors ($MAE = 3.56 Wm^{-2}$) (Garcia et al., in review). λE estimates from the more physically based two source model (TSM) (Norman et al., 1995) run with in-situ T_s from exactly the same dataset and aggregated at daily-time scale were also less accurate ($r^2 = 0.34–0.31$) than PT-JPL-daily run with in-situ or MSG T_s results (Morillas et al., in press) (Table 8). TSM results using separate measurements of soil and vegetation T_s instead of an aggregated measure did not improved the results (Morillas et al., in press).

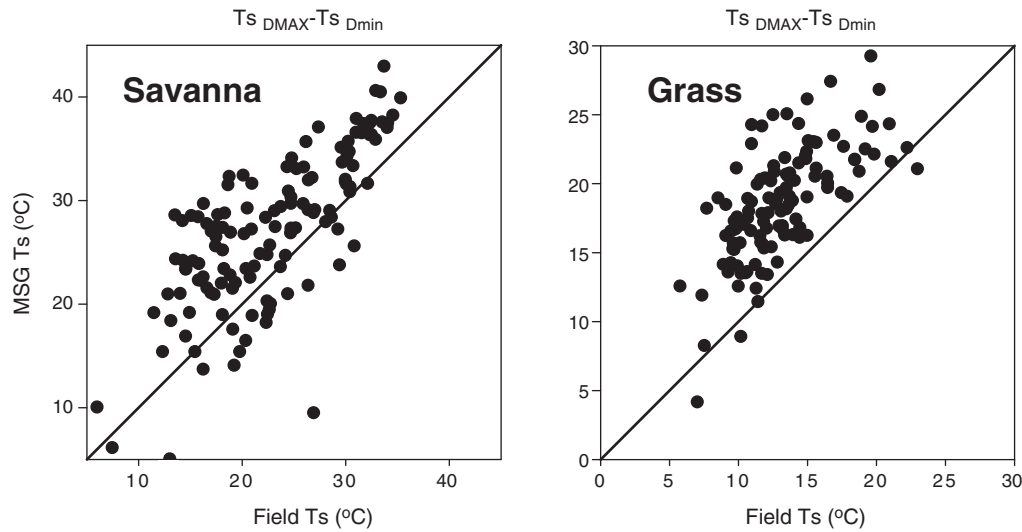


Fig. 7. Comparison of the diurnal surface temperature difference ($T_{sD_{MAX}} - T_{sD_{min}}$) from field (Apogee) and satellite (MSG–SEVIRI) sensors in the savanna and in the Mediterranean grassland.

Finally, to place the results from PT-JPL-daily ran with *ATI* in the context of global drylands, we compared them with studies using Penman–Monteith remote sensing (PM) or Priestley–Taylor (PT) models over savannas and grasslands at dryland sites from different regions of the globe (Table 8). These comparisons should always be considered with caution as each model uses different input data sources and both the environmental conditions and the vegetation change. However, we have focused on the less accurate PT-JPL-daily algorithm, amenable for regionalization ($FDa_{ATI-MSG}$) ran with satellite MSG and MODIS data both for vegetation and soil moisture constraints, leaving T_{air} and available energy as the only field input variables used.

It can be seen in Table 8 that PT-JPL-daily $FDa_{ATI-MSG}$ in the Sahelian savanna ($r^2 = 0.80$; $RMSE = 26.53 \text{ Wm}^{-2}$) performed better in general than PM models at other savanna sites although it has to be considered that not all these models were forced with local meteorological inputs (Table 8). Thus, the PML improved algorithm from Zhang et al. (2010) where maximum stomatal conductance is optimized with a hydro-meteorological model, showed lower r^2 at two Australian savannas ($r^2 = 0.53$ and 0.49) less arid than our site (with 1764 mm and 526 mm of annual rainfall respectively) with the PT-JPL-daily error within the range of those two sites (Table 8). Results from a PM

model in one of the Australian savannas forced with in-situ meteorological inputs were also poorer than our results ($r^2 = 0.23$) (Cleugh et al., 2007). Our algorithm performed also better than the MODIS product for evapotranspiration (MOD16) of Mu et al. (2011), in three woody savannas in arid regions of the USA (with r^2 ranging from 0.06 to 0.61). Again, PT-JPL-daily errors were within Mu et al. (2011) ranges of error at those savanna sites ($RMSE = 18.51\text{--}30.6 \text{ Wm}^{-2}$). In another global study Yuan et al. (2010) used a PM approach optimized with Eddy Covariance λE from 21 sites. Their model in the Mediterranean savanna of Tonzi performed worse (Table 8) than PT-JPL-daily using $f_{SM-ATI-MSG}$ in the Sahelian savannah although it should be noted that they used air temperature from reanalysis. In the same savanna of Tonzi ranch, Vinukollu et al. (2011) applied a daily version of the PT-JPL model with the soil moisture constraint based on the water vapor deficit although the error was low ($RMSE = 18.75 \text{ Wm}^{-2}$) the non-parametric Kendall's Tau (equivalent to Pearson-correlation coefficient) was 0.74 using only satellite input data.

Regarding the Mediterranean grassland site, our model λE results using satellite data for soil moisture and vegetation ($FDa_{ATI-MSG}$) ($r^2 = 0.32$; $RMSE = 15.03 \text{ Wm}^{-2}$) were in the range of the MOD16 algorithm of Mu et al. (2011) for two arid steppe grasslands in the USA with $r^2 = 0.48$ (Audubon) and 0.25 (Walnut Gulch) respectively

Table 7

Evaluation of PT-JPL-daily λE with Eddy Covariance data for different parameterizations of the soil moisture constraint derived from atmospheric water deficit: $f_{SM-Fisher} = RH^{VPD/\beta}$. Results are shown for midday and daily average conditions for *RH* (relative humidity) and *VPD* (Vapor Pressure Deficit) and for $\beta = 0.1 \text{ kPa}$ and $\beta = 1 \text{ kPa}$. Results from the best performing combination of parameters in each site are shown in bold font. In the savanna results were evaluated between June and December 2007 and in the Mediterranean grasslands from January to June 2011. Model versions starting with “*FDa*” were run with $f_{APAR-NDVI}$ and LAI_{NDVI} and with “*FDb*” with $f_{APAR-MODIS}$ and LAI_{MODIS} .

Site	Period	Conditions	β (kPa)	Model version	r^2	MAE	Bias	RMSE	MPE (%)
Savanna (Agoufou)	All dates	daily	1	FDa_{Fisher}	0.69	26.09	14.87	32.81	41.87
				FDb_{Fisher}	0.80	18.08	8.47	24.35	29.01
			0.1	FDa_{Fisher}	0.71	20.49	41.13	53.18	32.88
				FDb_{Fisher}	0.66	23.60	37.92	49.94	37.87
		Midday	1	FDa_{Fisher}	0.62	32.19	29.27	43.05	51.65
				FDb_{Fisher}	0.61	35.72	25.62	40.61	57.32
			0.1	FDa_{Fisher}	0.68	18.65	43.04	56.21	29.93
				FDb_{Fisher}	0.65	21.86	39.71	52.45	35.09
Mediterranean grasslands (Balsa Blanca)	Growing season	Daily	1	FDa_{Fisher}	0.16	15.08	−6.68	19.40	43.73
				FDb_{Fisher}	0.17	28.25	−26.38	34.44	81.89
			0.1	FDa_{Fisher}	0.36	21.22	8.49	14.74	66.67
				FDb_{Fisher}	0.27	20.40	9.49	16.24	64.10
		Midday	1	FDa_{Fisher}	0.16	35.03	−7.02	20.48	110.05
				FDb_{Fisher}	0.13	36.24	−8.23	21.92	113.87
			0.1	FDa_{Fisher}	0.64	14.42	15.61	18.23	45.30
				FDb_{Fisher}	0.53	12.24	17.92	20.66	38.44

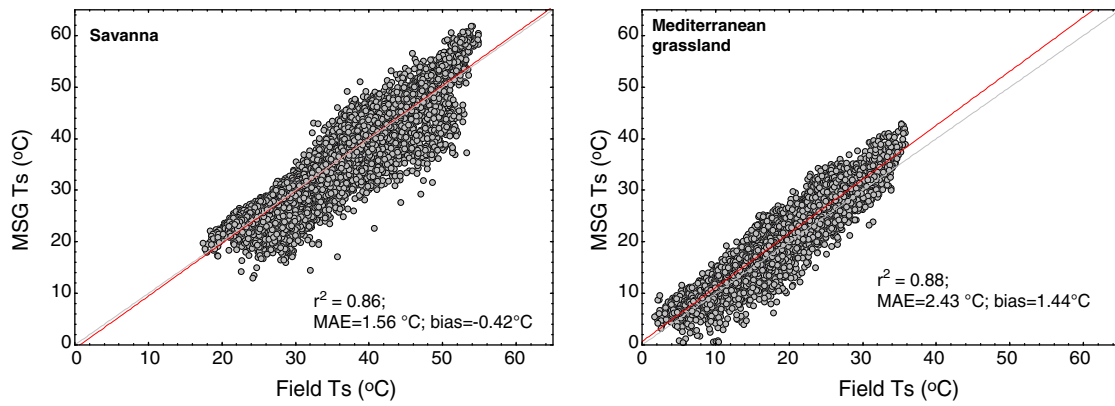


Fig. 8. Comparison of 15 minute observations of radiometric surface temperature from field (Apogee) and satellite (MSG-SEVIRI) sensors in the savanna and in the Mediterranean grassland during the study period.

Table 8

Statistics from actual evapotranspiration models using remote sensing data over dryland savanna and grassland sites. Climate classification is based on Köppen–Geiger (Kottek et al., 2006) where BWh: arid/desert/hot air; BSk: cold/semiarid, Aw: equatorial/desert; Csb: warm temperate/summer dry/warm summer; Cfb: warm temperate/fully humid/warm summer; Csa: warm temperate/summer dry/hot summer. A brief description of model type is included. When errors were reported in mm day⁻¹ they have been converted into Wm⁻². Statistics in parenthesis refer to the model type explanations in parenthesis.

Ecosystem type	Site	Country	Lat° Lon°	Climate type	Model type	r ²	MAE	RMSE	Reference
Open woody savanna	Sahel (Agoufou)	Mali	15.34, -1.48	BWh	PT-JPL-daily f_{SM-ATI} satellite (in-situ)	0.80 (0.83)	20.21 (19.72)	26.53 (23.10)	This study
Open woody savanna	Sahel (Agoufou)	Mali	15.34, -1.48	BWh	SVAT in-situ calibration	0.81	16.57	9.90	Ridler et al. (2012) ^a
Open woody savanna	Sahel (Agoufou)	Mali	15.34, -1.48	BWh	SVAT satellite calibration	0.63	39.24	46.66	Ridler et al. (2012) ^a
Open woody savanna	Sahel (Dahra)	Senegal	15.41 - 15.47	BWh	Triangle using SEVIRI/MODIS	0.75	-	31.00	Stisen et al. (2008)
Open woody savanna	Sahel (SD-DEM)	Sudan	13.28 - 0.48	BWh	Sim-ReSET using SEVIRI/MODIS	0.73	26.00	-	Sun et al. (2011)
Open woody savanna	Virginia Park	Australia	-19.88 146.55	Aw	PM- in situ meteorological	0.23	-	112.1	Cleugh et al. (2007)
Open woody savanna	Virginia Park	Australia	-19.88 146.55	Aw	PML-optimized with hydrol. model	0.49	-	15.94	Zhang et al. (2010)
Savanna	Howard Springs	Australia	-12.50° 131.15	Aw	PML-optimized with hydro. model	0.53	-	32.18	Zhang et al. (2010)
Woody savanna	AZ - Flagstaff - Wildfire	USA	35.40 - 111.80	Csb	MOD16. PM new version (old version)	0.06 (0.42)	-	23.92 (18.51)	Mu et al. (2011)
Woody savanna	TX -Freeman Ranch Mesquite Juniper	USA	29.9 - 98.0	Cfa	MOD16. PM new version (old version)	0.48 (0.52)	-	25.91 (30.76)	Mu et al. (2011)
Mediterranean savanna	CA - Tonzi Ranch	USA	38.4 - 121.0	Csa	MOD16. PM new version (old version)	0.61 (0.53)	-	19.08 (21.36)	Mu et al. (2011)
Mediterranean savanna	CA - Tonzi Ranch	USA	38.4 - 121.0	Csa	PM (field eddy calibration)	0.57	-	30.19	Yuan et al. (2010)
Mediterranean savanna	CA - Tonzi Ranch	USA	38.4	Csa	PT-JPL-daily	0.74 (Kendall)	-	19.39	Vinukollu et al. (2011)
Mediterranean grasslands	Balsa Blanca	Spain	36.94 - 2.03	BSk	PT-JPL-daily f_{SM-ATI} satellite (in-situ)	0.31 (0.57)	10.78 (11.44)	15.03 (10.96)	This study
Mediterranean grasslands	Balsa Blanca	Spain	36.94 - 2.03	BSk	PML-input SWC	0.54	13.03	-	Morillas et al. (2011), in review
Mediterranean grasslands	Balsa Blanca	Spain	36.94 - 2.03	BSk	PML-input rainfall (two methods)	0.32-0.47	13.88-9.92	-	Morillas et al. (2011), in review
Mediterranean grasslands	Balsa Blanca	Spain	36.94 - 2.03	BSk	Triangle using MODIS	0.24	3.56	-	Garcia et al. (in review)
Mediterranean grasslands	Balsa Blanca	Spain	36.94 - 2.03	BSk	TSM with Ts composite in parallel (series)	0.34 (0.31)	39.05 (53.82)	43.89 (58.52)	Morillas et al. (in press) ^a
Mediterranean grasslands	Balsa Blanca	Spain	36.94 - 2.03	BSk	TSM with Ts soil, Ts canopy in parallel (series)	0.14 (0.25)	44.86 (57.67)	51.00 (62.50)	Morillas et al. (in press) ^a
Arid steppe grasslands	AZ -Audubon Research Ranch	USA	31.6 - 110.5	BSk	MOD16. PM new version (old version)	0.22 (0.48)	-	23.07 (23.07)	Mu et al. (2011)
Arid steppe grasslands	AZ -Audubon Research Ranch	USA	31.6 - 110.5	BSk	PT-JPL-daily	0.37 (Kendall's)	-	18.75	Vinukollu et al. (2011)
Arid steppe grasslands	AZ - Walnut Gulch Kendall Grasslands	USA	31.7 - 109.9	BSk	MOD16. PM new version (old version)	0.07 (0.25)	-	19.36 (18.51)	Mu et al. (2011)
Mediterranean grassland	CA-Vairaranch	USA	38.40 - 120.95	Csa	PM (field eddy calibration)	0.51	-	-4.56	Yuan et al. (2010)

^a 30 minute model outputs provided by the authors have been aggregated to daily scale in this work to compare with the rest of the models.

with the old algorithm version and $r^2 = 0.05$ and 0.49 with the new version. Our PT-JPL-daily model errors were lower than Mu et al. (2011); RMSE = 22.95 and 18.42 Wm^{-2} with the old algorithm and RMSE = 22.95 and 19.26 Wm^{-2} with the new algorithm. In Audubon steppe the PT-JPL-daily model of Vinukollu et al. (2011) was not very successful in capturing the temporal dynamics (Kendall's Tau = 0.37) but showed still a better performance than Mu et al. (2011) algorithm ran during the same time (not shown in Table 8). Results from Yuan et al. (2010) PM model calibrated with field data at another Mediterranean grassland (Vairaranch) were better than our model results $r^2 = 0.51$ and bias = 0.16 Wm^{-2} .

5. Conclusions

The Priestley Taylor-Jet Propulsion Laboratory (PT-JPL) evapotranspiration λE model, developed by Fisher et al. (2008) is based on the Priestley–Taylor equation downscaled according to multiple stresses. The PT-JPL is attractive for its simplicity and potential for regionalization using satellite data. In this study, a daily version of the model was evaluated in some of the most extreme conditions from the point of water availability: an open woody savanna in the Sahel and a Mediterranean grassland, both with annual rainfall below 400 mm. A new approach was tested with in-situ and satellite data using a soil moisture constraint based on the apparent thermal inertia concept (f_{SM-ATI}) relying on remotely sensed observations of surface temperature and albedo.

When using field measured soil water content (SWC) to estimate the soil moisture constraint, the daily PT-JPL model reproduced the λE dynamics measured from Eddy Covariance systems within the uncertainty levels of the closure error system. When using the apparent thermal inertia index f_{SM-ATI} at the Sahelian savanna, results with in-situ data were equivalent to those obtained using field measured SWC. When up-scaling the f_{SM-ATI} to MSG–SEVIRI satellite data, a satisfactory agreement with field data was also found ($r^2 = 0.80$; MAE = 20.21 Wm^{-2}). At the Mediterranean grassland, results using f_{SM-ATI} were less accurate both for in-situ and satellite data ($r^2 = 0.57$ – 0.31 ; MAE = 9.85 – 10.78 Wm^{-2} respectively) but still outperformed reported results of two more complex models ran at the site: the two source model (TSM) and the Penman–Monteith–Leuning (PML) model.

In the context of global drylands, the PT-JPL λE model using f_{SM-ATI} provides results comparable in accuracy to more complex models at similar savanna and grassland biomes. Nonetheless, efforts should be made when using f_{SM-ATI} to reduce evapotranspiration overestimates when the soil is completely dry and to improve the cloud-mask algorithm as the f_{SM-ATI} is very sensitive to changes in solar irradiance.

This study also showed that the original model formulation for soil moisture constraint, f_{SM} , relying on the atmospheric water deficit should be calibrated differently in each site to obtain meaningful λE results. Therefore, the use of soil moisture constraints like ATI based on routinely available products like surface temperature or albedo or from soil moisture missions like the SMOS (Soil Moisture & Ocean Salinity mission) or the future NASA mission SMAP (Soil Moisture Active Passive) would eliminate the need of water vapor data and field site calibrations at dryland regions. The described modeling framework is also suitable for introducing information from spectral regions currently under-used in evapotranspiration models. For example, canopy water status could be tracked by shortwave infrared indices (Ceccato et al., 2002; Zarco-Tejada et al., 2003) and photosynthetic activity by narrow-band indices like the Photochemical Reflectance Index, PRI (Gamon et al., 1997; Peñuelas et al., 2011). Due to the strong coupling between evapotranspiration and carbon assimilation fluxes in dryland regions, some of the biophysical constraints used in this model could be used to regionalize Gross Primary Productivity (GPP) estimates based on Light Use Efficiency models.

Acknowledgments

This study was funded by the Danish Council for Independent Research and Technology and Production Sciences (FTP) Grant 09-070382, the research project RNM-6685 financed by the Regional Andalusian Government (Spain), and the CARBORAD project CGL2011-27493 (Plan Nacional MICINN, Spain). MODIS data were obtained through the online Data Pool at the NASA Land Processes Distributed Active Archive Center (LP DAAC), USGS/Earth Resources Observation and Science Center, Sioux Falls, South Dakota (http://lpdaac.usgs.gov/get_data). The authors would like to thank EUMETSAT for providing the MSG–SEVIRI data. Field data for the savanna site in Mali were collected within the frame of the AMMA project (www.amma-eu.org). The Malian site belongs to the AMMA-CATCH observatory (www.amma-catch.org). The authors acknowledge helpful comments and feedback from Mads Olander Rasmussen, Hector Nieto and Simon Proud. Manuscript review from Joshua Fisher and three other anonymous referees is gratefully acknowledged.

References

- Anderson, M. C., Norman, J. M., Mecikalski, J. R., Otkin, J. A., & Kustas, W. P. (2007). A climatological study of evapotranspiration and moisture stress across the continental United States based on thermal remote sensing: 2. Surface moisture climatology. *Journal of Geophysical Research-Atmospheres*, 112.
- Baldocchi, D. (2008). Breathing of the terrestrial biosphere: Lessons learned from a global network of carbon dioxide flux measurement systems. *Australian Journal of Botany*, 56, 1–26.
- Berni, J. A. J., Zarco-Tejada, P. J., Sepulcre-Canto, G., Fereres, E., & Villalobos, F. (2009). Mapping canopy conductance and CWSI in olive orchards using high resolution thermal remote sensing imagery. *Remote Sensing of Environment*, 113, 2380–2388.
- Boegh, E., Soegaard, H., & Thomsen, A. (2002). Evaluating evapotranspiration rates and surface conditions using Landsat TM to estimate atmospheric resistance and surface resistance. *Remote Sensing of Environment*, 79, 329–343.
- Bouchet, R. J. (1963). Evapotranspiration réelle et potentielle, signification climatique. *International Association of Hydrological Sciences (IAHS), Pub.*, 62, (pp. 134–142).
- Boulet, G., Chehbouni, A., Gentine, P., Duchemin, B., Ezzahar, J., & Hadria, R. (2007). Monitoring water stress using time series of observed to unstressed surface temperature difference. *Agricultural and Forest Meteorology*, 146, 157–172.
- Brogaard, S., Runnstrom, M., & Seaquist, J. (2005). Primary production of Inner Mongolia, China, between 1982 and 1999 estimated by a satellite data-driven light use efficiency model. *Global and Planetary Change*, 45, 313–332.
- Brownsey, G. J., Eldridge, J. W., Jarvis, D. A., Ross, G., & Sanders, I. (1976). New light-scattering photogoniometer for accurate measurements. *Journal of Physics E-Scientific Instruments*, 9, 654–658.
- Brutsaert, W. (1982). *Evaporation into the atmosphere—Theory, history, and application* (pp. 299). Dordrecht, Holland: D. Reidel Publishing Company.
- Cai, G., Xue, Y., Hu, Y., Wang, Y., Guo, J., Luo, Y., et al. (2007). Soil moisture retrieval from MODIS data in Northern China Plain using thermal inertia model. *International Journal of Remote Sensing*, 28, 3567–3581.
- Campbell, J. S., & Norman, N. J. (1998). *An introduction to environmental biophysics* (2nd ed.). Springer (Chapter 15).
- Campolongo, F. S. A., Sørensen, T., & Tarantola, S. (2000). Hitchhiker's guide to sensitivity analysis. *Sensitivity analysis* (pp. 15–47). New York: Wiley.
- Ceccato, P., Gobron, N., Flasse, S., Pinty, B., & Tarantola, S. (2002). Designing a spectral index to estimate vegetation water content from remote sensing data: Part 1—Theoretical approach. *Remote Sensing of Environment*, 82, 188–197.
- Chebouni, A., LoSeen, D., Njoku, E. G., Lhomme, J. P., Monteny, B., & Kerr, Y. H. (1997). Estimation of sensible heat flux over sparsely vegetated surfaces. *Journal of Hydrology*, 189, 855–868.
- Cleugh, H. A., Leuning, R., Mu, Q. Z., & Running, S. W. (2007). Regional evaporation estimates from flux tower and MODIS satellite data. *Remote Sensing of Environment*, 106, 285–304.
- Cracknell, A. P., & Xue, Y. (1996). Thermal inertia determination from space—A tutorial review. *International Journal of Remote Sensing*, 17, 431–461.
- Cukier, R. I., Levine, H. B., & Shuler, K. E. (1978). Nonlinear sensitivity analysis of multiparameter model systems. *Journal of Computational Physics*, 26, 1–42.
- de Rosnay, P., Gruhier, C., Timouk, F., Baup, F., Mougou, E., Hiernaux, P., et al. (2009). Multi-scale soil moisture measurements at the Gourma meso-scale site in Mali. *Journal of Hydrology*, 375, 241–252.
- Eagleson, P. S. (1986). The emergence of global-scale hydrology. *Water Resources Research*, 22, S6–S14.
- Fisher, J. B., Malhi, Y., Bonal, D., Da Rocha, H. R., De Araujo, A. C., Gamon, M., et al. (2009). The land-atmosphere water flux in the tropics. *Global Change Biology*, 15, 2694–2714.
- Fisher, J. B., Tu, K. P., & Baldocchi, D. D. (2008). Global estimates of the land-atmosphere water flux based on monthly AVHRR and ISLSCP-II data, validated at 16 FLUXNET sites. *Remote Sensing of Environment*, 112, 901–919.

- Gamon, J. A., Serrano, L., & Surfus, J. S. (1997). The photochemical reflectance index: an optical indicator of photosynthetic radiation use efficiency across species, functional types, and nutrient levels. *Oecologia*, *112*, 492–501.
- García, M., Oyonarte, C., Villagarcía, L., Contreras, S., Domingo, F., & Puigdefabregas, J. (2008). Monitoring land degradation risk using ASTER data: The non-evaporative fraction as an indicator of ecosystem function. *Remote Sensing of Environment*, *112*, 3720–3736.
- García, M., Were, A., Villagarcía, L., Fernandez, N., Domingo, F., Puigdefabregas, J., et al. (in review). Accuracy of a water deficit index derived from the NDVI-surface temperature relationship under water-limited or energy-limited conditions. *Remote Sensing of Environment*.
- Gillies, K. K., & Carlson, T. N. (1995). Thermal remote sensing of surface soil water content with partial vegetation cover for incorporation into climate models. *Journal of Applied Meteorology*, *34*, 745–756.
- Geiger, B., Carrer, D., Franchisteguy, L., Roujean, J. L., & Meurey, C. (2008). Land surface albedo derived on a daily basis from meteosat second generation observations. *IEEE Transactions on Geoscience and Remote Sensing*, *46*, 3841–3856.
- Giorgi, F., & Lionello, P. (2008). Climate change projections for the Mediterranean region. *Global and Planetary Change*, *63*, 90–104.
- Glenn, E. P., Huete, A. R., Nagler, P. L., Hirschboeck, K. K., & Brown, P. (2007). Integrating remote sensing and ground methods to estimate evapotranspiration. *Critical Reviews in Plant Sciences*, *26*, 139–168.
- Guichard, F., Kergoat, L., Mougín, E., Timouk, F., Baup, F., Hiernaux, P., et al. (2009). Surface thermodynamics and radiative budget in the Sahelian Gourma: Seasonal and diurnal cycles. *Journal of Hydrology*, *375*, 161–177.
- Houborg, R., Anderson, M. C., Norman, J. M., Wilson, T., & Meyers, T. (2009). Intercomparison of a 'bottom-up' and 'top-down' modeling paradigm for estimating carbon and energy fluxes over a variety of vegetative regimes across the U.S. *Agricultural and Forest Meteorology*, *149*(11), 1875–1895.
- Huete, A., Didan, K., Miura, T., Rodriguez, E. P., Gao, X., & Ferreira, L. G. (2002). Overview of the radiometric and biophysical performance of the MODIS vegetation indices. *Remote Sensing of Environment*, *83*, 195–213.
- Huntington, T. G. (2006). Evidence for intensification of the global water cycle: Review and synthesis. *Journal of Hydrology*, *319*, 83–95.
- Huxman, T. E., Wilcox, B. P., Breshears, D. D., Scott, R. L., Snyder, K. A., Small, E. E., et al. (2005). Ecohydrological implications of woody plant encroachment. *Ecology*, *86*, 308–319.
- Impens, I., & Lemeur, R. (1969). Extinction of net radiation in different crop canopies. *Archiv für Meteorologie, Geophysik und Bioklimatologie Serie B*, *17*, 403–412.
- Iqbal, M. (1983). *Introduction to solar radiation*. Toronto: Academic Press.
- Jarvis, P. G. (1976). Interpretation of variations in leaf water potential and stomatal conductance found in canopies in field. *Philosophical Transactions of the Royal Society of London. Series B, Biological Sciences*, *273*, 593–610.
- June, T., Evans, J. R., & Farquhar, G. D. (2004). A simple new equation for the reversible temperature dependence of photosynthetic electron transport: A study on soybean leaf. *Functional Plant Biology*, *31*, 275–283.
- Kelliher, F. M., Leuning, R., Raupach, M. R., & Schulze, E. D. (1995). Maximum conductances for evaporation from global vegetation types. *Agricultural and Forest Meteorology*, *73*, 1–16.
- Kottek, M., Grieser, J., Beck, C., Rudolf, B., & Rubel, F. (2006). World map of the Köppen-Geiger climate classification updated. *Meteorologische Zeitschrift*, *15*, 259–263.
- Kowalski, A. S., Anthoni, P. M., Vong, R. J., Delany, A. C., & Maclean, G. D. (1997). Deployment and evaluation of a system for ground-based measurement of cloud liquid water turbulent fluxes. *Journal of Atmospheric and Oceanic Technology*, *14*, 468–479.
- Kustas, W. P., & Norman, J. M. (1999). Evaluation of soil and vegetation heat flux predictions using a simple two-source model with radiometric temperatures for partial canopy cover. *Agricultural and Forest Meteorology*, *94*, 13–29.
- Leuning, R., Zhang, Y. Q., Rajaud, A., Cleugh, H., & Tu, K. (2008). A simple surface conductance model to estimate regional evaporation using MODIS leaf area index and the Penman-Monteith equation. *Water Resources Research*, *44*.
- Lu, S., Ju, Z., Ren, T., & Horton, R. (2009). A general approach to estimate soil water content from thermal inertia. *Agricultural and Forest Meteorology*, *149*, 1693–1698.
- Matsushita, B., Xu, M., Chen, J., Kameyama, S., & Tamura, M. (2004). Estimation of regional net primary productivity (NPP) using a process-based ecosystem model: How important is the accuracy of climate data? *Ecological Modelling*, *178*, 371–388.
- McMillen, R. T. (1988). An Eddy-Correlation technique with extended applicability to non-simple terrain. *Boundary-Layer Meteorology*, *43*, 231–245.
- Minacapilli, M., Iovino, M., & Blanda, F. (2009). High resolution remote estimation of soil surface water content by a thermal inertia approach. *Journal of Hydrology*, *379*, 229–238.
- Miralles, D. G., Holmes, T. R. H., De Jeu, R. A. M., Gash, J. H., Meesters, A. G. C. A., & Dolman, A. J. (2011). Global land-surface evaporation estimated from satellite-based observations. *Hydrology and Earth System Sciences*, *15*, 453–469.
- Mitra, D. S., & Majumdar, T. J. (2004). Thermal inertia mapping over the Brahmaputra basin, India using NOAA-AVHRR data and its possible geological applications. *International Journal of Remote Sensing*, *25*, 3245–3260.
- Monteith, J. L. (1972). Solar radiation and productivity in tropical ecosystems. *Journal of Applied Ecology*, *9*, 747–766.
- Moran, S. M., Clarke, T. R., Inoue, Y., & Vidal, A. (1994). Estimating crop water deficit using the relationship between surface-air temperature and spectral vegetation index. *Remote Sensing of Environment*, *49*, 246–263.
- Morillas, L., Uclés, O., Sanchez-Cañete, E. P., García, M., Villagarcía, L., & Domingo, F. (2011). Improving evapotranspiration estimates in semiarid ecosystems: The role of soil evaporation. *Abstract presented at the 12th European Ecological Federation Congress, Ávila (Spain) 25–29 September*.
- Morillas, L., Leuning, R., Villagarcía, L., García, M., Serrano-Ortiz, P., & Domingo, F. (in review). Improving evapotranspiration estimates in Mediterranean drylands: the role of soil evaporation. *Water Resources Research*.
- Morillas, L., García, M., Nieto, H., Villagarcía, L., Sandholt, I., Gonzalez-Dugo, M.P., et al. (in press). Using radiometric surface temperature for energy flux estimation in Mediterranean drylands from a two-source perspective. *Remote Sensing of Environment*.
- Morton, F. I. (1983). Operational estimates of areal evapotranspiration and their significance to the science and practice of hydrology. *Journal of Hydrology*, *66*, 1–76.
- Mougín, E., Hiernaux, P., Kergoat, L., Grippe, M., de Rosnay, P., Timouk, F., et al. (2009). The AMMA-CATCH Gourma observatory site in Mali: Relating climatic variations to changes in vegetation, surface hydrology, fluxes and natural resources. *Journal of Hydrology*, *375*, 14–33.
- Mu, Q. Z., Heinsch, F. A., Zhao, M., & Running, S. W. (2007). Development of a global evapotranspiration algorithm based on MODIS and global meteorology data. *Remote Sensing of Environment*, *111*, 519–536.
- Mu, Q. Z., Zhao, M. S., & Running, S. W. (2011). Improvements to a MODIS global terrestrial evapotranspiration algorithm. *Remote Sensing of Environment*, *115*, 1781–1800.
- Myneni, R. B., Hoffman, S., Knyazikhin, Y., Privette, J. L., Glassy, J., Tian, Y., et al. (2002). Global products of vegetation leaf area and fraction absorbed PAR from year one of MODIS data. *Remote Sensing of Environment*, *83*, 214–231.
- Myneni, R. B., & Williams, D. L. (1994). On the relationship between FAPAR and NDVI. *Remote Sensing of Environment*, *49*, 200–211.
- Nearing, G. M., Moran, M. S., Scott, R. L., & Ponce-Campos, G. (2012). Coupling diffusion and maximum entropy models to estimate thermal inertia. *Remote Sensing of Environment*, *119*, 222–231.
- Nemani, R. R., & Running, S. W. (1989). Estimation of regional surface-resistance to evapotranspiration from NDVI and thermal-IR AVHRR data. *Journal of Applied Meteorology*, *28*, 276–284.
- New, M., Hulme, M., & Jones, P. (2000). Representing twentieth-century space-time climate variability. Part II: Development of 1901–96 monthly grids of terrestrial surface climate. *Journal of Climate*, *13*, 2217–2238.
- Nicholson, S. (2000). Land surface processes and Sahel climate. *Reviews of Geophysics*, *38*, 117–139.
- Nishida, K., Nemani, R., Running, S., & Glassy, J. (2000). An operational remote sensing algorithm of land surface evaporation. *Journal of Geophysical Research, D: Atmospheres*, *108* (Art. 4270).
- Norman, J. M., Kustas, W. P., & Humes, K. S. (1995). Source approach for estimating soil and vegetation energy fluxes in observations of directional radiometric surface-temperature. *Agricultural and Forest Meteorology*, *77*, 263–293.
- Overgaard, J. (2005). Energy-based land-surface modelling: new opportunities in integrated hydrological modelling. PhD Thesis. Lyngby: Institute of Environment and Resources, Technical University of Denmark.
- Peñuelas, J., Garbulsky, M. F., & Filella, I. (2011). Photochemical reflectance index (PRI) and remote sensing of plant CO₂ uptake. *New Phytologist*, *191*, 596–599.
- Potter, C. S., Randerson, J. T., Field, C. B., Matson, P. A., Vitousek, P. M., Mooney, H. A., et al. (1993). Terrestrial ecosystem production—a process model-based on global satellite and surface data. *Global Biogeochemical Cycles*, *7*, 811–841.
- Price, J. C. (1977). Thermal inertia mapping: A new view of the earth. *Journal of Geophysical Research*, *82*, 2582–2590.
- Priestley, C. H. B., & Taylor, R. J. (1972). On the assessment of surface heat flux and evaporation using large-scale parameters. *Monthly Weather Review*, *100*, 81–92.
- Qiu, G. Y., Shi, P. J., & Wang, L. M. (2006). Theoretical analysis of a remotely measurable soil evaporation transfer coefficient. *Remote Sensing of Environment*, *101*, 390–398.
- Rey, A., Belleli-Marchesini, L., Were, A., Serrano-Ortiz, P., Etiopie, G., Papale, D., et al. (2012). Wind as a main driver of the net ecosystem carbon balance of a semiarid Mediterranean steppe in the South East of Spain. *Global Change Biology*, *18*, 539–554.
- Ridler, M. E., Sandholt, I., Butts, M., Lerer, S., Mougín, E., Timouk, F., et al. (2012). Calibrating a soil-vegetation-atmosphere transfer model with remote sensing estimates of surface temperature and soil surface moisture in a semi arid environment. *Journal of Hydrology*, *436–437*, 1–12.
- Ross, J. (1976). Radiative transfer in plant communities. In J. L. Monteith (Ed.), *Vegetation and the atmosphere* (pp. 13–56). London: Academic Press.
- Saltelli, A., Tarantola, S., & Chan, K. P. S. (1999). A quantitative model-independent method for global sensitivity analysis of model output. *Technometrics*, *41*, 39–56.
- Sandholt, I., Rasmussen, K., & Andersen, J. (2002). A simple interpretation of the surface temperature/vegetation index space for assessment of surface moisture status. *Remote Sensing of Environment*, *79*, 213–224.
- Saux-Picart, S., Otle, C., Perrier, A., Decharme, B., Coudert, B., Zribi, M., et al. (2009). SEtHyS_Savannah: A multiple source land surface model applied to Sahelian landscapes. *Agricultural and Forest Meteorology*, *149*, 1421–1432.
- Schmetz, J., Pili, P., Tjemkes, S., Just, D., Kerkmann, J., Rota, S., et al. (2002). An introduction to Meteosat Second Generation (MSG). *Bulletin of the American Meteorological Society*, *83*, 977–+.
- Schymanski, S. J., Sivapalan, M., Roderick, M. L., Hutley, L. B., & Beringer, J. (2009). An optimality-based model of the dynamic feedbacks between natural vegetation and the water balance. *Water Resources Research*, *45*.
- Shuttleworth, W. J., & Wallace, J. S. (1985). Evaporation from sparse crops—An energy combination theory. *Quarterly Journal of the Royal Meteorological Society*, *111*, 839–855.
- Sobrino, J. A., El Kharraz, M. H., Cuenca, J., & Raissouni, N. (1998). Thermal inertia mapping from NOAA-AVHRR data. *Synergistic use of multisensor data for land processes*, *22*, 655–667.
- Stisen, S., Jensen, K., Sandholt, I., & Grimes, D. (2008). A remote sensing driven distributed hydrological model of the Senegal River basin. *Journal of Hydrology*, *354*, 131–148.
- Sun, Z., Gebremichael, M., Ardö, J., & de Bruin, H. A. R. (2011). Mapping daily evapotranspiration and dryness index in the East African highlands using MODIS and SEVIRI data. *Hydrology and Earth System Sciences*, *15*, 163–170.

- Taylor, C. M., Gounou, A., Guichard, F., Harris, P. P., Ellis, R. J., Couvreux, F., et al. (2011). Frequency of Sahelian storm initiation enhanced over mesoscale soil-moisture patterns. *Nature Geoscience*, 4, 430–433.
- Timouk, F., Kergoat, L., Mougou, E., Lloyd, C. R., Ceschia, E., Cohard, J. M., et al. (2009). Response of surface energy balance to water regime and vegetation development in a Sahelian landscape. *Journal of Hydrology*, 375, 178–189.
- Tramutoli, V., Claps, P., Marella, M., Pergola, N., & Sileo, C. (2000). Feasibility of hydrological application of thermal inertia from remote sensing. *2nd Plinius Conference on Mediterranean Storms, 16–18 Siena, Italy*.
- Trigo, I. F., Peres, L. F., DaCamara, C. C., & Freitas, S. C. (2008). Thermal land surface emissivity retrieved from SEVIRI/Meteosat. *IEEE Transactions on Geoscience and Remote Sensing*, 46, 307–315.
- Twine, T. E., Kustas, W. P., Norman, J. M., Cook, D. R., Houser, P. R., Meyers, T. P., et al. (2000). Correcting eddy-covariance flux underestimates over a grassland. *Agricultural and Forest Meteorology*, 103, 279–300.
- Van Doninck, J., Peters, J., De Baets, B., De Clercq, E. M., Ducheyne, E., & Verhoest, N. E. C. (2011). The potential of multitemporal Aqua and Terra MODIS apparent thermal inertia as a soil moisture indicator. *International Journal of Applied Earth Observation and Geoinformation*, 13, 934–941.
- Verhoef, A. (1998). The relative importance of surface and aerodynamic resistances in a multi-source energy-CO₂ model. *Physics and Chemistry of the Earth*, 23, 459.
- Verstraeten, W. W., Veroustraete, F., & Feyen, J. (2006a). On temperature and water limitation of net ecosystem productivity: Implementation in the C-Fix model. *Ecological Modelling*, 199, 4–22.
- Verstraeten, W. W., Veroustraete, F., van der Sande, C. J., Grootaers, I., & Feyen, J. (2006b). Soil moisture retrieval using thermal inertia, determined with visible and thermal spaceborne data, validated for European forests. *Remote Sensing of Environment*, 101, 299–314.
- Vinukollu, R. K., Wood, E. F., Ferguson, C. R., & Fisher, J. B. (2011). Global estimates of evapotranspiration for climate studies using multi-sensor remote sensing data: Evaluation of three process-based approaches. *Remote Sensing of Environment*, 115, 801–823.
- Wan, Z. M., & Dozier, J. (1996). A generalized split-window algorithm for retrieving land-surface temperature from space. *IEEE Transactions on Geoscience and Remote Sensing*, 34, 892–905.
- Webb, E. K., Pearman, G. I., & Leuning, R. (1980). Correction of flux measurements for density effects due to heat and water-vapor transfer. *Quarterly Journal of the Royal Meteorological Society*, 106, 85–100.
- Were, A., Villagarcia, L., Domingo, F., Alados-Arboledas, L., & Puigdefabregas, J. (2007). Analysis of effective resistance calculation methods and their effect on modelling evapotranspiration in two different patches of vegetation in semi-arid SE Spain. *Hydrology and Earth System Sciences*, 11, 1529–1542.
- Yuan, W. P., Liu, S. G., Yu, G. R., Bonnefond, J. M., Chen, J. Q., Davis, K., et al. (2010). Global estimates of evapotranspiration and gross primary production based on MODIS and global meteorology data. *Remote Sensing of Environment*, 114, 1416–1431.
- Zarco-Tejada, P. J., Rueda, C. A., & Ustin, S. L. (2003). Water content estimation in vegetation with MODIS reflectance data and model inversion methods. *Remote Sensing of Environment*, 85, 109–124.
- Zhang, Y. Q., Chiew, F. H. S., Zhang, L., Leuning, R., & Cleugh, H. A. (2008). Estimating catchment evaporation and runoff using MODIS leaf area index and the Penman-Monteith equation. *Water Resources Research*, 44, W10420.
- Zhang, K., Kimball, J. S., Mu, Q., Jones, L. A., Goetz, S. J., & Running, S. W. (2009). Satellite based analysis of northern ET trends and associated changes in the regional water balance from 1983 to 2005. *Journal of Hydrology*, 379, 92–110.
- Zhang, Y., Leuning, R., Hutley, L. B., Beringer, J., McHugh, I., & Walker, J. P. (2010). Using long-term water balances to parameterize surface conductances and calculate evaporation at 0.05° spatial resolution. *Water Resources Research*, 46.